

Shaped Ultrafast Optical Pumping for NMR Applications

by

Jason Matthew Taylor

B.E. Electrical Engineering, Physics and Mathematics
Vanderbilt University (1999)

Submitted to the Program in Media Arts and Sciences,
School of Architecture and Planning
in partial fulfillment of the requirements for the degree of

Master of Science in Media Arts and Sciences

at the

MASSACHUSETTS INSTITUTE OF TECHNOLOGY

June 2002

©Massachusetts Institute of Technology, 2002

Author
Program in Media Arts and Sciences,
School of Architecture and Planning
May 10, 2002

Certified by
Neil Gershenfeld
Associate Professor
Thesis Supervisor

Accepted by
Andrew B. Lippman
Chairperson, Departmental Committee on Graduate Students

Shaped Ultrafast Optical Pumping for NMR Applications

by

Jason Matthew Taylor

Submitted to the Program in Media Arts and Sciences,
School of Architecture and Planning
on May 10, 2002, in partial fulfillment of the
requirements for the degree of
Master of Science in Media Arts and Sciences

Abstract

High polarization of nuclear spin systems is essential for quantum information processing using nuclear magnetic resonance and for sensitive spectroscopic measurements. Unfortunately for liquids, the polarization of such systems is terribly small— $O(10^{-5})$. Continuous Wave (CW) optical pumping can increase the polarization of simple systems. For sufficiently complicated molecules, determining a pumping scheme analytically is intractable.

Recent experiments have shown that shaped ultrafast laser pulses controlled by machine learning algorithms has promise for solving previously unapproachable problems in physical chemistry. Shaped light has been used to break specific bonds in molecules and drive chemical reactions.

We investigate the potential of enhancing nuclear spin polarization in liquid NMR through the application of shaped ultrafast laser pulses. The excited-singlet \rightarrow ground-triplet transition intersystem crossing is mediated by spin-orbit coupling of the molecule. Shaped ultrafast pumping has revolutionized control of the wavefunctions of electrons of molecules [Zew00]. The main body of this work is a review of the fields related to shaped ultrafast optical pumping and NMR.

Presented here is a proposal for a set of experiments to investigate the usefulness of shaped ultrafast optical pumping for NMR applications. This document begins with a pedagogical review of relevant material. Then proceeds to discuss an experimental exploration of the space around this research trajectory. We then propose a set of experiments to test the feasibility of shaped ultrafast optical pumping, and then present some preliminary results.

Thesis Supervisor: Neil Gershenfeld

Title: Associate Professor

Acknowledgments

I thank my parents and brother for their love and support.

I would also like to thank Jojo for her love and friendship.

I thank Neil Gershenfeld for his support, advice and insight. He is responsible for everything I know about spin. Ike Chuang is intense. I'm extremely happy that he decided to join us here at the lab. His advice in the 11th hour of this thesis is appreciated.

I thank our University of Michigan collaborators Phil Bucksbaum and his student Daniel Morris. Daniel has spent many long hours in the laser lab on this project including several days introducing me to their lab. Thanks Brett for your help over there.

I would like to thank both of my undergraduate advisors, Sandra Rosenthal for her close mentoring of me in my first research group and Len Feldman for instilling in me a deep fondness for the element Silicon. Joe Jacobson had some great ideas regarding this thesis and pointed me in this direction.

Yael was exceedingly helpful to me in my first two years at the lab. Working with him on the development of the table-top NMR was a pleasure. I thank my group mates, Rehmi, Matt, Ben V., Rich, Esa, Dan, Caroline. It's been an adventure writing a thesis with Ben Recht on my right side for the last two months, he helped me out quite a bit with a few details and put up pretty well with me continuously talking about singlet to triplet transitions. It's a good thing that this is a large office.

Tadd Kippeny from my old group at Vanderbilt has been a dear friend of mine for years. As far as this thesis goes, it's nice that he has almost completed a Ph.D. in Physical Chemistry using Ultrafast Lasers. His words of wisdom and rigorous thinking really helped me understand this field much better.

I would like to thank Hui-Hui for his contribution of a poem to my thesis. I think that it improves this document quite a bit.

Ike's group was a great help in working on the experimental sections of this thesis.

Matthias Steffen was great with his NMR. Aram Harrow made some of the best corrections to this thesis, and Andrew Houck had some words on optics. There are many people around the lab that keep this place running. Thanks Susan, Michael, Linda, Pat and Liz. Not much would get done around here with out you. Many graduate students and research scientists around the lab have been very helpful, Brian Chow, Steve Smith, David Mosley.

Shaped Ultrafast Optical Pumping for NMR Applications

by

Jason Matthew Taylor

Submitted to the Program in Media Arts and Sciences,
School of Architecture and Planning

in partial fulfillment of the requirements for the degree of
Master of Science in Media Arts and Sciences

at the

MASSACHUSETTS INSTITUTE OF TECHNOLOGY

June 2002

Thesis Advisor.....
Neil Gershenfeld
Associate Professor
Program in Media Arts and Sciences, Physics and Media
MIT

Thesis Reader
Isaac Chuang
Associate Professor
Program in Media Arts and Sciences, quanta
MIT

Thesis Reader
Philip Bucksbaum
Professor
Physics Department, Randall Laboratory
University of Michigan

ELECTRICAL PROBLEM AT THE HIGH SCHOOL PROM

Already they were moving into
the crowd, barely confident in their
white suits, each one hoping to be
mistaken for another in the darkness:

like watching chickens hatch
more chickens, the egg-shells
twitching, and how dizzy they
must feel like before they emerge:

so the men's heads were set spinning
by the scent of the gardenias,
the corsages that dropped petals
on the floor in a jumble of night,
legs, and more night:

warm and amniotic as sweat.
But when the sound system began
to fail after the first act & they
brought in the electricians to root

out the thing inside that wailed
like a baby when the air pressure
changes we heard a loud pop and
then the lights went on:

that cold and fluent light that we felt
as a rock edged against our bodies.
It was as if we had been undressed
by strangers, it was as if Vesuvius

had just erupted. One girl jerked
her hands out from where they were
not meant to be: suddenly it was gym
class. We all moved quickly to line
up against the wall.

Tung-Hui Hu

Contents

1	Introduction	10
1.1	Moore's Law and Quantum Computers	11
1.2	Motivation	13
1.3	Prior Art	14
1.4	Goals	14
1.5	Closing thought	15
2	Spectroscopy, Spin and Optical Pumping	16
2.1	Atomic Spectroscopy	16
2.1.1	Angular Momentum of Two Electrons	17
2.1.2	The Singlet and Triplet State	19
2.2	L-S Coupling	20
2.2.1	Hyperfine Coupling	20
2.2.2	The Zeeman effect	20
2.2.3	Fine Structure	21
2.3	Electronic Molecular Spectroscopy	21
2.3.1	Chemistry Notation	21
2.3.2	Basic Bonds	22
2.4	Inter-System Crossing	22
2.4.1	Phosphorescence	23
3	NMR: T_1, T_2, T_2^*, INEPT, ENDOR, and all that...	26
3.1	The Nucleus	26
3.2	Spin Polarization	27
3.2.1	T_1	28

3.3	Bloch Vector Description	28
3.3.1	T_2, T_2^* and the Spin Echo	31
3.4	NMR Pulse Sequences	32
3.4.1	FID from a 90 pulse	32
3.4.2	IR: Inversion Recovery measures T_1	32
3.4.3	CPMG measures T_2	33
3.5	Spin-Spin Coupling	33
3.5.1	J-coupling and Dipolar Coupling	33
3.6	Tensor Product Operator Formalism	33
3.6.1	Multiple Spins	36
3.7	The Hamiltonian	37
3.8	A quick bit of Quantum	38
3.9	Hartman-Hahn Condition	39
3.9.1	ENDOR	39
3.9.2	INEPT	41
3.9.3	COSY and NOESY	41
3.10	DNP	42
3.11	CIDNP	42
3.12	MIONP	43
4	Genetic Algorithms	45
4.1	Algorithm Setup	46
4.2	Basic Algorithm	46
5	Experimental Exploration	49
5.1	Electronics	49
5.1.1	NMR spectrometers	50
5.1.2	FPGAs and Verilog	51
5.1.3	Boards	52
5.2	NMR Systems	55
5.2.1	Table top magnet	55
5.2.2	Halbach Cylinder NMR	57
5.2.3	Electromagnet	60

5.2.4	500 MHz and 200 MHz Superconducting Magnet	61
5.3	1 μmol of Photons	62
5.3.1	Photon Budget	62
5.3.2	Magnets	62
5.3.3	Boltzmann Sample Polarization	63
5.3.4	Coumarin 500 ($\text{C}_{12}\text{H}_{10}\text{NO}_2\text{F}_3$)	64
5.3.5	NMR of Flourine	66
5.3.6	Hydrogen might be better	67
6	Proposal for Experiments	70
6.1	Maximize Absorption of Angular Momentum	71
6.2	Nuclear Spin Polarization	71
6.2.1	Light vs. Dark NMR signal	72
6.3	Electron Spin Angular vs Orbital Angular Momentum	73
6.3.1	Phosphorescence	73
6.4	Electron Polarization Transfer to Nuclear Spin	73
7	Preliminary Results	75
7.1	Absorption of Angular Momentum	75
7.1.1	The Laser	75
7.1.2	The GA	76
7.1.3	Experiment: Max. Absorption of Angular Momentum	77
7.1.4	Pump Probe Setup	77
7.2	Progress and Results	83
7.2.1	Results: Maximize Absorption of Angular Momentum	83
8	Conclusions	90
A	MO Simulation	91
B	Derivations with Spin	96
B.1	Spin Operators	96
B.2	Two $\frac{1}{2}$ Spins	97
B.2.1	Clebsch-Gordan Coefficients	98

B.3	spin $\frac{1}{2}$	99
B.4	Spin in a magnetic field	99
B.5	The Larmor Precession	100
C	Glossary	102

Chapter 1

Introduction

The Boltzmann nuclear spin polarization at thermal equilibrium is unacceptable for many NMR applications.

Quantum computers in nuclear magnetic resonance (NMR) systems are limited by polarization. The complexity of the problem that can be approached is limited by the number of qubits available. Using current experimental techniques each additional qubit for room temperature liquid NMR requires exponentially more polarization [War97]. Although the cost now can be made polynomial [SV98], we still need polarization enhancement to make the prefactor reasonable.

Also, the sensitivity of NMR spectroscopy is limited by the amount of spin polarization. Traditionally the way to improve this polarization is to increase magnetic field strength. Currently the most sensitive NMR spectrometers have twenty-one Tesla fields and require a large lab space. At a price tag of around \$2 million, they have reached both financial and physical limits.

Near unity polarization of nuclear spin in atoms has been demonstrated [SPHR99] via continuous wave (CW) optical pumping. This relies on pumping specific absorption lines of atoms in the gas phase. In these simple atomic systems, the dynamics of electron and nuclear interaction is well understood. For sufficiently complicated molecules, selecting an arbitrary transition is analytically intractable. Narrow frequency CW optical pumping is sufficient for pumping simple molecules. For molecules with many atoms using fine time-frequency control of the shape of the pump pulse to control the quantum states of the molecule is promising [RdVRMK00].

In recent years, much attention has been given to ultrafast lasers for controlling molecular dynamics. In 1999 Ahmed Zewail received the Nobel Prize in Chemistry for Femtochemistry [Zew00]. Femtosecond ultrafast-lasers can establish coherent states across the molecule. This light can break specific bonds and drive chemical reactions.

We have begun investigating the feasibility of using shaped ultrafast lasers to increase nuclear polarization in molecules. We believe that a circularly polarized shaped ultrafast pulse alone, or possibly in conjunction with an electron spin resonance (ESR) pulse, will increase nuclear polarization. Before jumping immediately into nuclear polarization, we attempted to maximize the absorption of angular momentum by the molecule using shaped pulses. Much effort has also been spent in preparation for the nuclear polarization experiment—the low sample concentration required for optical feedback makes NMR detection non-trivial.

1.1 Moore’s Law and Quantum Computers

The current trend of miniaturization of chip design to improve performance will plateau sometime in the next two decades. At current rates, transistors shortly will consist of only a few atoms and the cost of a fabrication lab will top \$1 trillion [WC98]. Quantum effects will begin to dominate technologists’ concerns as the quest for a smaller chip is continued. Microchip design is ill equipped to handle the problems that await. Totally new approaches will be required. One of the most exciting is quantum computing.

Quantum computing changes the way problems of computation and information handling are solved on the most basic level. Typically a quantum computer is made of many two level systems, or “qubits”. The ability to perform arbitrary single qubit operations and the ability to perform a CNOT gate on any of two qubits is required to make a quantum computer.

In 1995, Peter Shor devised a quantum algorithm to efficiently factor large numbers [Sho95]. Because the popular RSA encryption technique assumes that factoring large integers is computationally hard, a quantum computer, able to factor large numbers exponentially faster than a digital computer, would render that encryption standard useless. A number of algorithms for solving other problems with a quantum computer have been proposed. Grover’s search algorithm [Gro97b], when presented with unsorted data, can interrogate multiple data points simultaneously. A classical computer would need to check each possibility in-

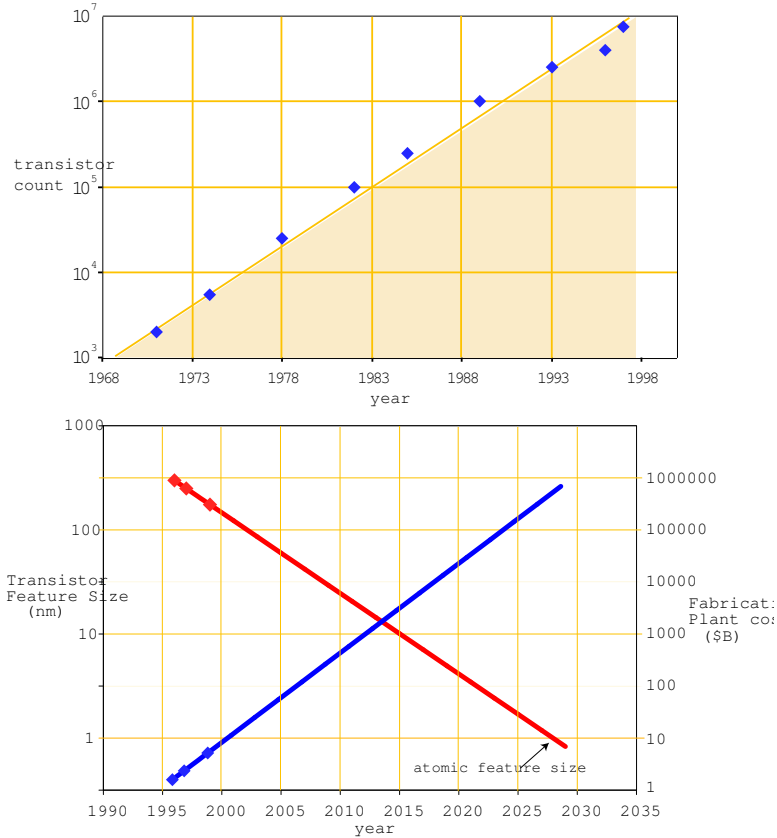


Figure 1-1: The trend of transistor count and feature sizes follows an exponential [Moo65]. Data updated from www.intel.com.

dividually. For a large database, Grover proposed [Gro97a] that it is possible to search an arbitrarily large unsorted database in $O(\sqrt{N})$ steps.

Many physical systems have been proposed for use as a quantum computer. A good review of the requirements for physical implementation can be found in chapter 7 of Nielsen and Chuang [NC00]. We are interested in quantum computing with NMR. In Nuclear Magnetic Resonance Quantum Computing (NMRQC) the states addressed are the spin of the nuclei in a molecule. NMR has long coherence time ($\approx 1-2$ secs) due to the electrons shielding the nuclei, but unfortunately not enough signal strength for a large quantum computer.

Nuclear magnetic resonance is a powerful tool for determining molecular structure. By establishing a strong, homogeneous, magnetic field through a sample and using a radio frequency (RF) generated electromagnetic field to address the spins of specific nuclei in atoms in molecules, one may input a number frequencies and obtain a resonance spectrum

that is generally unique to each molecule. Nuclear spins in molecules can be strongly coupled through chemical bonds to other nuclei in the same molecule.

Using this system as a quantum computer, a given molecule has a set of spins or qubits, that can be manipulated by a series of RF pulses. With coherence times of up to several seconds, there is enough time to initialize a state, apply the algorithm, and read the result.

In 1998, Isaac Chuang, Neil Gershenfeld, and Mark Kubinec implemented the first two bit quantum computer [CGK98]. Their NMRQC performed Grover’s search algorithm required technically fewer steps than a classical computer. In one iteration, the NMRQC was able to find the desired bit. A classical digital computer would require 2.25 compares. The Deutsch-Jozsa quantum algorithm was also implemented in 1998 on a NMRQC [CVZ⁺98]. This algorithm determines if an unknown function has all zeros, all ones, or an equal number of zeros and ones as members. A classical computer would require up to $2^{N-1} + 1$ function calls to determine this condition, where N is the number of bits. A quantum computer was able to accomplish this task with one iteration for N=2. In 2000, Vandersypen et. al. [VSB⁺00] demonstrated an experimental realization of exponential speedup over a classical computer by implementing an order-finding algorithm. The structure of the order-finding algorithm was the same as Shor’s algorithm. These implementations using a NMRQC are examples of the simplest cases of the respective algorithms.

1.2 Motivation

In an NMR quantum computer attaining only a small number of qubits, around 6-10, has been called “dauntingly” difficult [War97]. Given a sufficient increased polarization of the nuclear spins NMR quantum computing may become useful [War97].

For all of its successes NMR is fairly insensitive in the low polarization limit. Biological molecules require averaging for many hours to get sufficient signal to noise for structural determination. Increasing spin polarization of a molecule would reduce the averaging time required. If this research direction converges on a route to increased polarization and the method is not prohibitively expensive, then integration with less expensive NMR systems may allow for more widespread use of NMR.

1.3 Prior Art

Optical Pumping of gases with circularly polarized light can result in increased polarization of atoms [Cor77, WH97, Hap72]. In this process angular momentum is transferred from the photons to the atoms. The efficiency can be quite high resulting in hyperpolarized noble gasses that can be used to enhance medical imaging techniques [CS01].

High proton nuclear spin has been achieved at 77 Kelvin in pentacene via DNP. Using microwave radiation a new record has been set for polarization enhancement [ITS⁺00]. In that process a laser is used to excite a pair of electrons into an excited-singlet state. An intersystem crossing allows for the conversion into a triplet state. In pentacene we have a non uniform distribution among the m_s states of the triplet. This allows for a microwave saturation of a transition to result in increased electron polarization. This leads to increased nuclear polarization via DNP.

Experiments over the last few years have shown that shaped ultrafast laser pulses controlled by machine learning algorithms have promise for discovering solutions to problems thought analytically impossible [PWWB01].

1.4 Goals

Given the tremendous success of optical pumping in the gas phase and the encouraging results of increased polarization in other systems, we expect that a novel pulse shape of circularly polarized light from an ultrafast laser will allow us to transfer angular momentum into the molecule and eventually the nuclear spin.

The first goal of this thesis is to present a survey of fields related to using shaped ultrafast lasers for increasing polarization in NMR systems. We begin with a pedagogical review of relevant material and then present some experimental exploration. The second goal is to propose a set of experiments to investigate the usefulness of shaped ultrafast optical pulses for NMR applications. In Chapter 7 we present some encouraging preliminary results—these experiments are the first of those proposed in Section 6.1.

1.5 Closing thought

Shaped ultrafast pumping of molecules with NMR readout has many exciting prospects. This thesis represents the beginning of a long term research agenda. The scope of this project is well beyond a masters thesis and may consume one or two doctoral students.

Chapter 2

Spectroscopy, Spin and Optical Pumping

Here we will review the basics of atomic and molecular spectroscopy. The final sections will examine Inter-System Crossings and DNP.

2.1 Atomic Spectroscopy

We'll begin with a review of atomic spectroscopy. This section will be helpful review when discussing CW optical pumping and will serve as the starting point for Electronic Molecular Spectroscopy.

The Pauli exclusion principle states that no two electrons in an atom can have the same quantum number. By using a few selection rules emission and absorption lines can be predicted. We must always conserve angular momentum. This section followed Corney [Cor77] and Krane [Kra96].

The angular momentum quantum number is usually referred to by (s,p,d,f,g,h) for values (0,1,2,3,4,5). So, for a particular orbital angular momentum l the total number of electrons allowed is $2(2l + 1)$.

For the Bohr atom the energy levels are:

$$E_n = -\frac{me^4}{32\pi^2\epsilon_0^2\hbar^2} \frac{1}{n^2}$$

where n is the principal quantum number.

- [n] principal quantum number: $n = 1,2,3,4\dots$
- [l] orbital angular momentum: $l = 0,1,2,3,\dots,n-1$
- [m_l] total angular momentum: $m_l = 0,\pm 1,\pm 2,\dots,\pm l$
- [m_s] electron spin: $m_s = \pm \frac{1}{2}$

Figure 2-1: Quantum Numbers for an Electron

H	$1s^1$
He	$1s^2$
Li	$1s^2 2s^1$
Be	$1s^2 2s^2$
B	$1s^2 2s^2 2p^1$
Ne	$1s^2 2s^2 2p^6$
Ar	$[\text{Ne}] 3s^2 3p^6$
Kr	$[\text{Ar}] 4s^2 3d^{10} 4p^6$
Xe	$[\text{Kr}] 5s^2 4d^{10} 5p^6$

Figure 2-2: Element Electronic Configuration

The four quantum numbers of a particular electron fully defines its state. Atomic spectroscopy observes the allowed transitions between states. The selection rules are arrived at by conserving angular momentum.

$$\Delta l = \pm 1$$

There is no selection rule for n .

2.1.1 Angular Momentum of Two Electrons

It is important to conserve angular momentum. We will now review how two electrons in the valence shell of an atom add angular momentum. We will follow the development in Kane [Kra96] for this section. This section will be important for the later review of how angular momentum works in chemical bonds.

For two electrons in the valence orbital of an electron we can add the orbital angular momentum of each electron.

$$L = L_1 + L_2$$

The L vectors must conform to the following rules:

$$\begin{aligned}L_{max} &= l_1 + l_2 \\L_{min} &= |l_1 - l_2|\end{aligned}\tag{2.1}$$

L must be an integer value.

$$M_L = m_{l1} + m_{l2}$$

The values of M_L can go from $-L$ to L inclusive with integer steps.

The \vec{S} spin angular momentum vector is created by adding the two electron spins. Since $m_s = \pm\frac{1}{2}$, S must be either 1 or 0.

Hund's Rule

In order to find the ground state of the two electrons we need to apply Hund's rule.

Find these two values but do not violate the Pauli principle. First:

$$S = M_{S,max}$$

Then:

$$L = M_{L,max}$$

Ground State of Carbon

To find the ground state of Carbon we can apply Hund's rules. For Carbon there are two 2p electrons in the valence shell. The $M_{S,max}$ value will be 1 since the electrons can both have values of $m_s = \frac{1}{2}$. $M_{L,max}$ must also be 1 since $l = 1$ and therefore $m_l = 1$ for one electron and $m_l = 0$ for the other. So the ground state of carbon is $S = 1$ $L = 1$.

To have a transition from state to another then these selection rules must be obeyed:

$$\Delta L = 0, \pm 1$$

and

$$\Delta S = 0$$

2.1.2 The Singlet and Triplet State

The first excited state for Helium is $1s2s$. We have two allowed combinations of L and S . $L = 0, S = 0$ and $L = 0, S = 1$. The former corresponds to a single allowed state of the electrons' spins anti-aligned. Where the $L = 0, S = 1$ allows for three M_S values of $-1, 0, 1$. The $L = 0, S = 0$ is called a singlet state and the $L = 0, S = 1$ is called a triplet state. The difference between these two states is some energy and one unit of angular momentum.

The actual states correspond to these wave functions: For $|S, M_S\rangle$. The three states with $S=1$

$$\begin{aligned} |1, 1\rangle &= \uparrow\uparrow \\ |1, 0\rangle &= \frac{1}{\sqrt{2}}(\uparrow\downarrow + \downarrow\uparrow) \\ |1, -1\rangle &= \downarrow\downarrow \end{aligned} \tag{2.2}$$

and one state with $S=0$:

$$|0, 0\rangle = \frac{1}{\sqrt{2}}(\uparrow\downarrow - \downarrow\uparrow) \tag{2.3}$$

The three states are called triplet states and the $S=0$ state is called a singlet.

In section B.2 a derivation of a triplet and singlet state is given. That derivation assumes an atom of one proton and one electron. For hydrogen, the energy difference between the triplet and singlet state is 5.88×10^{-6} eV. This corresponds to a frequency of 1420 MHz. The wavelength is 21cm. This is the same 21cm line of Hydrogen that astronomers love.

The triplet state is usually a metastable state. Since the transition to the singlet ground state will require a $\Delta S = 1$ then that transition is "forbidden". This implies that it the transition will take a long time relative to allowed transitions. Typical times for each might be 20ns for allowed transitions and $20\mu\text{secs}$ for forbidden ones.

2.2 L-S Coupling

L-S Coupling is sometimes called Russell-Saunders coupling or spin-orbit coupling.

$$\vec{J} = \vec{L} + \vec{S}$$

2.2.1 Hyperfine Coupling

Up to this point, we have neglected the nuclear magnetic moment. The nuclear magnetic moment will be discussed at length in Chapter 3. For the purposes of introducing hyperfine coupling we will assume that the nucleus has a spin of $\frac{1}{2}$.

The nuclear magnetic moment is,

$$\vec{\mu}_I = \gamma\mu_N\vec{I}$$

where the nuclear magneton $\mu_N = \frac{e\hbar}{2M_p}$.

Our Hamiltonian for the interaction will be just the dot product of \vec{I} and \vec{J} . This is sometimes called spin-spin coupling.

$$H_{spin-spin} = A_J\vec{I} \cdot \vec{J}$$

The A_J is the strength of the hyperfine coupling.

2.2.2 The Zeeman effect

In the absence of a magnetic field and ignoring spin, the energy levels depend on only n . The energy levels for all combinations of the other quantum numbers would be degenerate.

In the presence of a magnetic field, the magnetic moment $\vec{\mu}_l$ associated with the orbital angular momentum interacts with the field.

$$E = -\vec{\mu}_l \cdot \vec{B} = \mu_l B_0$$

$$\mu_l = m_l \mu_B$$

Where μ_B is the Bohr magneton $\mu_B = \frac{e\hbar}{2m}$. The energy splitting is known as the Zeeman effect. For a p orbital there will be three values of $m_l = 0, \pm 1$ and the energy difference will

be $\Delta E = \mu_B B_0$.

2.2.3 Fine Structure

The two angular momentum vectors \vec{L} and \vec{S} can be either aligned or anti-aligned. This corresponds to a difference of energy. In hydrogen the energy is:

$$\Delta E = (mc^2)\alpha^4 \frac{1}{n^5} \approx 10^{-5} (\text{for } n = 2)$$

The fine structure constant α is

$$\alpha = \frac{e^2}{4\pi\epsilon_0\hbar c} \approx \frac{1}{137}$$

2.3 Electronic Molecular Spectroscopy

In molecular spectroscopy we still must obey the Pauli exclusion principle for each electron from a particular atom. The same rules for adding angular momentum of electrons on the same atom still apply.

2.3.1 Chemistry Notation

The sigma molecular orbital σ involves two s electrons or 1 s and 1 p . The sigma orbitals are symmetric around the plane of the molecule. A σ^* denotes a σ antibond.

Pi π orbitals are antisymmetric to the plane of the molecule. Two π bonds can form between two atoms along with a σ bond to make a triple bond.

$\pi \rightarrow \sigma^*$ denotes an electronic transition of a π bond to a σ^* anti-bond. $S_0 \rightarrow S_n$ denotes a singlet ground state to singlet excited state transition. The UV-Vis absorption spectra is made of these transitions.

A n bond is a “bond” for two electrons on the same atom. They’re more commonly called lone pairs.

Highest Occupied Molecular Orbital (HOMO) and Lowest Unoccupied Molecular Orbital (LUMO) are terms that are used to specify the position of where an excited electron would come from and go to in a particular electronic transition. In a double bond of a σ bond and a π bond, neither the σ or π bond are necessarily preferred to be the HOMO state, the HOMO is determined by the energy levels of each bond.

2.3.2 Basic Bonds

Figure 2-3 shows a sigma bond arising from two 1s atomic orbitals. The σ orbital is the bonding orbital and the σ^* is the antibonding orbital.

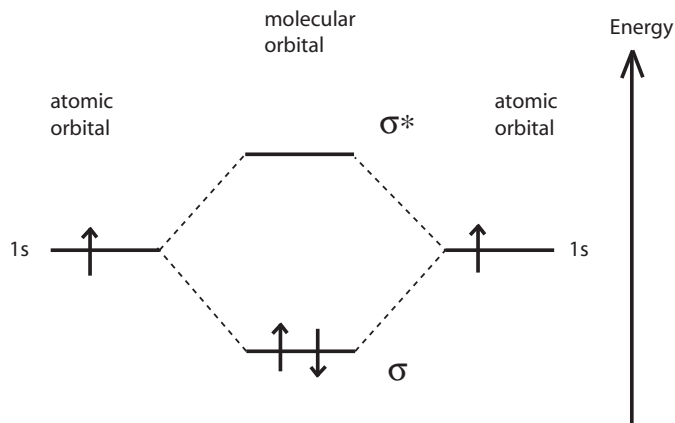


Figure 2-3: The Sigma Bond. H-H

The $\sigma \rightarrow \sigma^*$ transition obeys the

$$\Delta L = 0, \pm 1$$

and

$$\Delta S = 0$$

rules.

The sigma bond can be of a s and p orbital or of a s and s orbital. Figure 2-4 shows the molecular orbitals of HF. The F has two lone pairs in the 1s and 2s orbitals and one electron from the 2p orbital to the 1s orbital of Hydrogen.

2.4 Inter-System Crossing

Inter-System crossings (ISC) occur when the excited state of a molecule transfers from the singlet state to the triplet state. The triplet state has one unit of angular momentum. Couplings between triplet states and nuclear spin are discussed in Section 3.12. The singlet

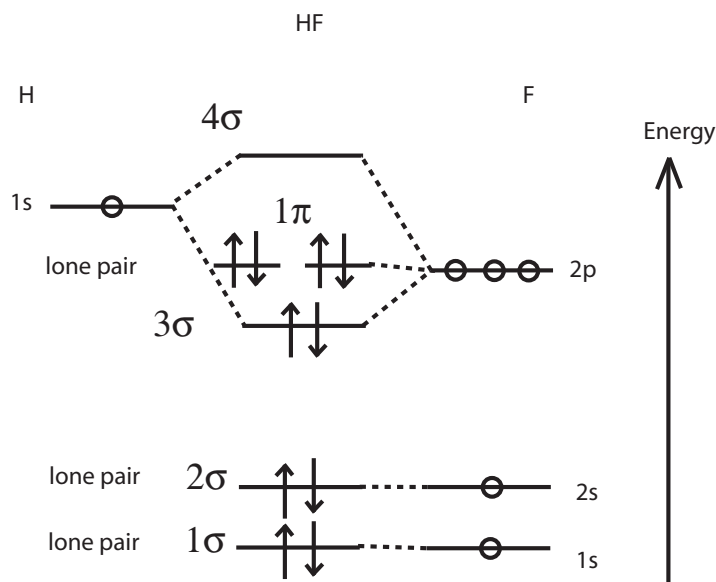


Figure 2-4: HF molecular orbital [HB89].

to triplet transition corresponds to

$$S = 0 \rightarrow S = 1.$$

This is a “forbidden” process. The triplet states are usually long lived due to the fact that it also “forbidden” to cross back to the singlet state. The singlet and triplet here are of electron spin; the wave-functions are the same as equations 2.2 and 2.3.

The rate of ISC can be increased by in the presence of paramagnetic or heavy atoms [HB89]. ISCs are also increased in the presence of O_2 .

Figure 2-5 is a chart from a paper [IAK00] on Time-Resolved Electron Spin Resonance (TRESR) of a variety of Porphyrins. The paper builds on previous work that indicates, “the photophysical properties of porphyrin complexes are controlled by spin-orbit coupling (SOC) of the central atom and axial ligand, which stimulates ISC.” This and related papers merit further study.

2.4.1 Phosphorescence

Phosphorescence in molecules happens when an electron in a bond is excited to a long lived metastable state and then does a radiative transition to the ground state. The long

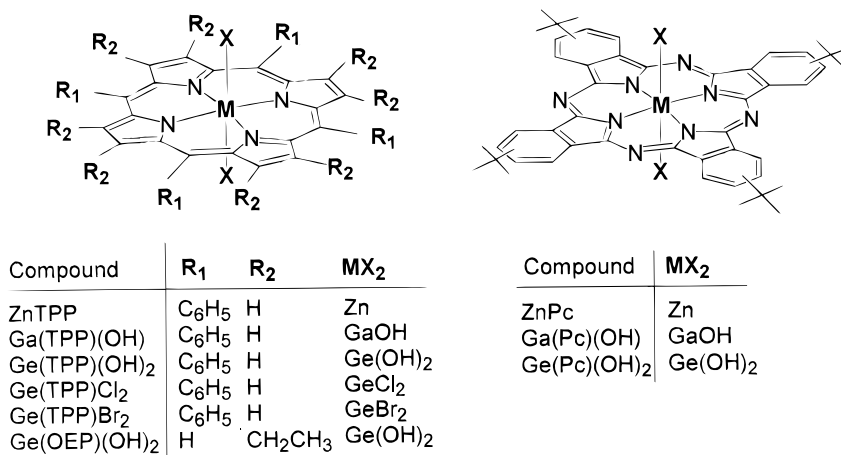


Figure 2-5: Porphyrin Studied in Time Resolved ESR ISC article. Image from [IAK00]

lived state is typically a triplet state. Figure 2-6 is a diagram of the transitions related to phosphorescence. The singlet-triplet transition occurs either because of spin-orbit ($L \cdot S$) coupling or vibrational modes. A molecule that exhibits phosphorescence may be a good choice for our system. It should be easy measure the singlet-triplet transition by watching the amount of phosphorescence.

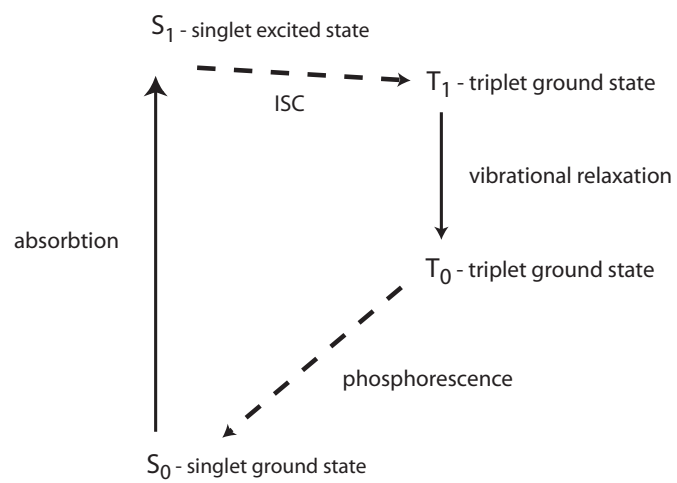


Figure 2-6: Phosphorescence

Chapter 3

NMR: T_1 , T_2 , T_2^* , INEPT, ENDOR, and all that...

In this chapter we introduce Nuclear Magnetic Resonance Spectroscopy (NMR). Nuclear spin transitions are proportional to the strength of the magnetic field. The Larmor resonance frequency is different for each atomic species. In the 50 or so years since NMR was discovered [PTP46], it has developed into a large field. Active research into both NMR techniques and applications is present in Physics, Chemistry, Biology and Medical Science [CS01].

There are many good experimental books [FR81, CP97, CAGPFS96]. Theoretical treatments can be found in books [EBW97] and review articles [SEL⁺83].

3.1 The Nucleus

Molecules are made of atoms. Atoms have nuclei. Nuclei sometimes have spin. Specifically, nuclei are made of protons and neutrons each has an intrinsic $\frac{1}{2}$ spin. The nucleons generally pair up and down. The result will be a net spin of zero, an integer spin, or a half-integer spin. This resulting spin is the nuclear angular momentum, I .

For non-zero I there will be a nuclear magnetic moment, μ :

$$\mu = \gamma \hbar I$$

where γ is the gyromagnetic ratio for a particular atom.

Nuclei	Unpaired Protons	Unpaired Neutrons	Net Spin	MHz/T
^1H	1	0	$\frac{1}{2}$	42.58
^2H	1	1	1	6.54
^{31}P	0	1	$\frac{1}{2}$	17.25
^{23}Na	2	1	$\frac{3}{2}$	11.27
^{14}N	1	1	1	3.08
^{13}C	0	1	$\frac{1}{2}$	10.71
^{19}F	0	1	$\frac{1}{2}$	40.08
^{129}Xe	0	1	$\frac{1}{2}$	11.78

Figure 3-1: Table of common NMR nuclei [Hor97b].

For, $\frac{1}{2}$ net spin nuclei placed in a magnetic field B_0 , the will net spin be either aligned (\uparrow) or anti-aligned (\downarrow) with the field. This corresponds to an energy difference:

$$U = \vec{\mu} \cdot \vec{B}$$

$$U = -\frac{1}{2}\gamma B_0 \hbar = \hbar\omega = h\nu$$

For Hydrogen, ν will be 42.58 MHz/Tesla. In a 11.8 T magnet, the Larmor resonant frequency for the Hydrogen transition is 500 MHz.

3.2 Spin Polarization

At equilibrium, in a reasonable magnetic field at room temperature, only a small number of nuclear spins will be polarized in the field.

The Hamiltonian determines the dynamics of the spins polarized by the magnet. A fairly small number of spins will be polarized in the magnetic field. This population inversion will be:

$$\epsilon = \frac{\mu B_0}{kT}$$

At $T = 300\text{K}$, $B_0 = 11.8\text{T}$, and μ for Hydrogen, we'll have an inversion on the order of 10^{-5} . The rest of the spins on the molecules will be aligned and anti-aligned resulting in a net-magnetization of zero.

The behavior of these spins will be dominated by the tendency of the system to, obey the 2nd law of thermodynamics and go towards thermodynamic equilibrium. The available

relaxation pathways of an excited spin will determine its behavior.

3.2.1 T_1

T_1 is the time constant for a NMR molecule to go to thermal equilibrium.

Molecules with a long T_1 are not very coupled to their environment. Two ways that nuclear spins usually couple to the environment is via electron spin coupling or by a RF at the Larmor frequency.

Because the spins used in NMR are reasonably decoupled from the environment, when they are in an excited state relative to thermal equilibrium, they will stay in that state for a fairly long time compared to systems better coupled to the environment. Typical T_1 values are 100ms or 1 second.

A quick way to observe a change in T_1 due to coupling to the environment is to put paramagnetic particles in an NMR sample. The spins in the sample will couple to the paramagnetic particles via dipolar coupling and, thus have a stronger coupling to the environment. The spins will relax to a ground state more quickly (T_1 will be shorter).

We are primarily concerned with liquid samples. Solids need to be spun in order to average out dipolar coupling terms. The rotational motion in a liquid does this naturally.

3.3 Bloch Vector Description

The Bloch vectors gives us a good way to think about NMR initially. A single spin molecule is completely described by the Bloch vector. Multiple spins will require a product operator description.

Figure 3-2 shows a basic NMR spectrometer. For the moment we will ignore the parts on the right and focus on the probe and sample geometry on the left.

We could imagine that addressing the $\approx 10^{23}$ nuclear spins behaves as if there were one large spin in the sample. This single magnetic moment is usually described as a magnet spinning around at the Larmor frequency. For a single spin, this fiction works out well.

If, as in the Figure 3-2, there is a coil around the sample aligned at 90 degrees to the large magnetic field, then, by turning on current in the coil we can induce a second magnetic field. By oscillating the current we can create a changing magnetic field. If we oscillate the current at the frequency at which the magnet spins, then we can flip the spinning magnet

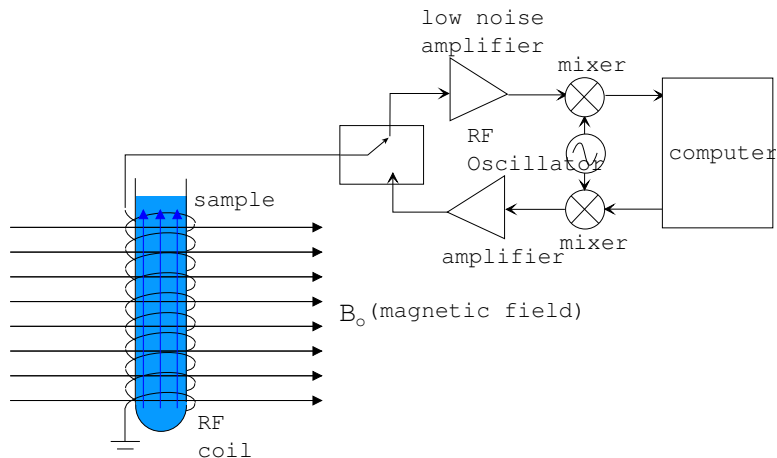


Figure 3-2: NMR Spectrometer diagram

onto its side. Matching the frequencies is called hitting a resonance.

The angle that the spin flips to is controlled by the product of the strength of coil magnetic field and the time that the field is left on. The time that the field is left on is called the pulse width. The pulse width is described by the angle that the spins flip to. A 90 degree pulse (or $\frac{\pi}{2}$ pulse) will turn the spinning magnet into the plane 90 degrees to the large magnetic field.

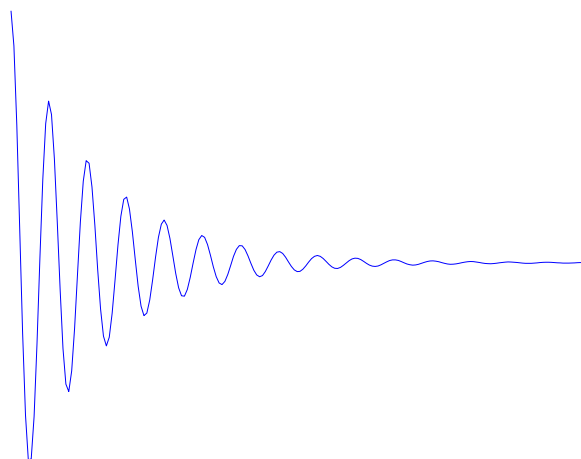


Figure 3-3: Free Induction Decay (FID)

Since an oscillating current in the coil made the spinning magnet flip over, then if we listen to the coil after doing a 90 (degree) pulse, then we should hear a signal coming back from the spinning magnet. This is in fact the case. Figure 3.3 shows the signal that we see coming back from the spinning magnet. The signal is called the Free Induction Decay or FID.

At this point we will dispense with the fiction that we are dealing with a single spinning magnet. The signal that we see coming back from the spinning magnet doesn't fit with that description. We will now introduce a new fiction. Rather than have one large spin, we will think about having 10^{23} spins each behaving just like the large single spin already discussed.

In addition to seeing an oscillating signal at the Larmor frequency, there is also an exponentially decaying envelope on the signal. One might assume—incorrectly—that this is due the spins returning to thermal equilibrium in fact, this is not the case. The spins do not all spin at exactly the same frequency. The effect of this is quantified in the numbers T_2 and T_2^* .

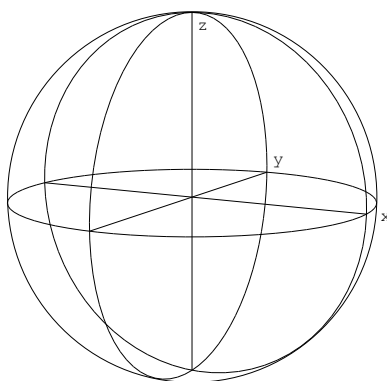


Figure 3-4: Bloch sphere

Before explaining why T_2 and T_2^* exist, we will describe how the spins appear to evolve.

The Bloch vector is used to describe how the spins evolve. The Bloch vector is described by these equations [Hor97a],

$$\begin{aligned}\frac{dM_{x'}}{dt} &= (\omega_0 - \omega)M_{y'} - \frac{M_{x'}}{T_2} \\ \frac{dM_{y'}}{dt} &= -(\omega_0 - \omega)M_{x'} + 2\pi\gamma B_1 M_z - \frac{M_{y'}}{T_2} \\ \frac{dM_z}{dt} &= -2\pi\gamma B_1 M_{y'} - \frac{(M_z - M_{z_0})}{T_1}\end{aligned}$$

where M is the spin magnetization, γ is the gyromagnetic ratio, and B_1 is the magnet's magnetic field.

T_2 and T_2^* is the observed decoherence in the rotating frame of the spins.

The observed signal in the coil is proportional to the magnitude of the magnetization

in the XY plane, M_x .

3.3.1 T_2 , T_2^* and the Spin Echo

In a Cartesian coordinate system where Z is aligned with the large magnetic field, the XY plane is where a single spin represented classically rotates at the Larmor frequency. In a 1 Tesla magnetic field the Larmor frequency for ^1H is 42.58 MHz. A 90° (or $\frac{\pi}{2}$ pulse) at the Larmor frequency will push the spins over into the XY plane. Interactions which reduce the magnitude of the Bloch vector in the XY plane are contained in T_2^* . T_2 is spin-spin dephasing and T_2^* is T_2 plus the effect of inhomogeneous magnetic fields.

As the spins become out of phase with each other the amplitude of the Bloch vector in the XY plane decreases. The faster rotating spins are moving ahead of the slower rotating spins and so the total vector sum of all of the spins is decreasing.

The Spin Echo

If, starting from thermal equilibrium, we hit the spins with a 90° pulse then we will observe the FID (figure 3.3). After waiting some time τ we can then hit the spins with a 180° pulse. We then observe an echo as shown in figure 3.3.1.

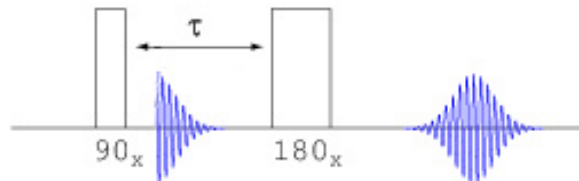


Figure 3-5: Spin Echo pulse sequence and responses

The spins have come back from somewhere. The 90° pulse put the spins into the plane of the coil and then they decohered as evidenced by the observation of the FID. After the 180° pulse the spins recohered and then decohered again. The 180° degree pulse flipped all of the spins around the center and so the slower spins were ahead of the faster spins. As the faster spins caught up the signal recohered and then continued to decohere again.

3.4 NMR Pulse Sequences

The single 90 pulse to get a FID and the spin echo are examples of some simple pulse sequences that can be done.

3.4.1 FID from a 90 pulse

We do pulse sequences to get information about the sample. In even a one spin system, the FID contains quite a bit of information. Specifically Larmor frequency and the profile of the FID. The Larmor frequency is directly proportional to the strength of the magnetic field. This means that an NMR FID, for a known nuclei, makes a very sensitive magnetometer. The shape of the FID will give us a measure of T_2^* , but more importantly we can get a measure of the homogeneity of the magnetic field. The practice of shimming a magnetic field uses the shape of a simple FID.

3.4.2 IR: Inversion Recovery measures T_1

We can use Inversion recovery to measure T_1 . Do a 180, wait τ then do a 90 and measure.

$$M = M_0(1 - 2 \exp(-\frac{\tau}{T_1}))$$

Do multiple experiments and vary τ , fit the data to this

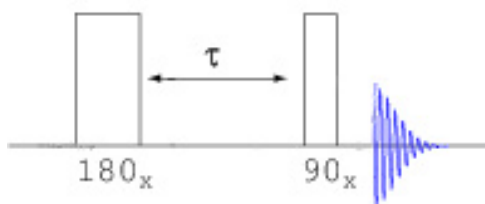


Figure 3-6: IR pulse sequence

$$M(\tau) = M_0(1 - 2 \exp(-\frac{\tau}{T_1}))$$

to find T_1 .

3.4.3 CPMG measures T_2

CPMG stands for Carr Purcell Meiboom Gill. In order to measure T_2 do a 90_x , then wait τ and do a 180_x . Acquire the max amplitude of the resulting spin echo. Then wait another τ and then do another 180_x and wait for the echo. Repeat until no signal is left.

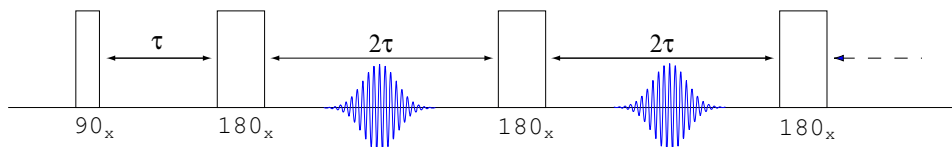


Figure 3-7: CPMG pulse sequence

Fit the results to this equation and solve for T_2 .

$$M(\tau) = M_0 \left(-\exp\left(\frac{\tau}{T_2}\right) \right)$$

3.5 Spin-Spin Coupling

NMR would be far less interesting without spin-spin coupling. Generally in NMR, we are concerned with nuclear spin to nuclear spin coupling. In this thesis we will also be interested in electron spin to nuclear spin hyperfine coupling.

3.5.1 J-coupling and Dipolar Coupling

J-coupling is a scalar coupling between two nuclei. The coupling is mediated by the chemical bonds of the NMR molecule. By looking at the splittings caused by J-coupling, it is usually possible to determine which atoms are bonded. Dipolar coupling is the through space coupling. It is usually much weaker than J coupling and of course falls off as a r^6 .

3.6 Tensor Product Operator Formalism

The density matrix and product operators allow us to describe accurately systems of multiple spins. The density matrix is used to predict observables.

There are many books that are good for this. In this section we will be following the development in a particularly helpful book [CAGPFS96]. For product operators Ernst has a good article [SEL⁺83].

We'll begin with the Pauli spin matrices in SU(2):

$$I_x = \frac{1}{2} \begin{bmatrix} 0 & 1 \\ 1 & 0 \end{bmatrix}$$

$$I_y = \frac{1}{2} \begin{bmatrix} 0 & -i \\ i & 0 \end{bmatrix}$$

$$I_z = \frac{1}{2} \begin{bmatrix} 1 & 0 \\ 0 & -1 \end{bmatrix}$$

$$[I_x, I_y] = iI_z$$

True under cyclic permutation of x, y, z .

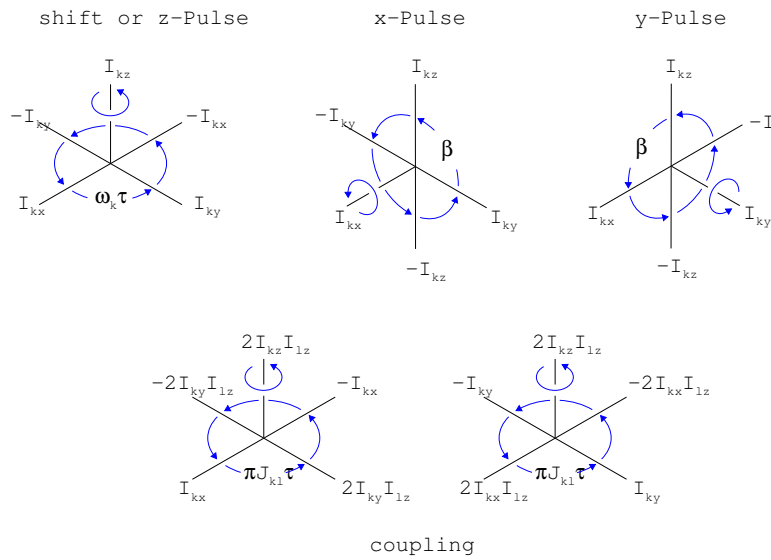


Figure 3-8: Product Operators [EBW97]

$$|\alpha\rangle = \begin{bmatrix} 1 \\ 0 \end{bmatrix} = |0\rangle$$

$$|\beta\rangle = \begin{bmatrix} 0 \\ 1 \end{bmatrix} = |1\rangle$$

An arbitrary ket is:

$$|\Phi\rangle = a|\alpha\rangle + b|\beta\rangle$$

From any basis we can go to any other via unitary transformations.

$$H = -\vec{\mu} \cdot \vec{B}t = H_z + H_{rf}$$

$$H = \omega_0 I_z + \omega_1 [I_x \cos(\omega_{rf}t + \phi) + I_y \sin(\omega_{rf}t + \phi)]$$

where $\omega_0 = -\gamma B_0$ and $\omega_1 = -\gamma B_1$.

We can then choose a unitary matrix to take us into the rotating frame of the spin.

$$U = \exp(i\omega_{rf}I_z t)$$

We then will have an effective Hamiltonian:

$$H_e = \omega_0 I_z + \omega_1 (I_x \cos \phi + I_y \sin \phi) - \omega_{rf} I_z = (\omega_0 - \omega_{rf}) I_z + \omega_1 (I_x \cos \phi + I_y \sin \phi) \quad (3.1)$$

This is the evolution of the density operator in the rotating frame.

If $\omega_0 - \omega_{rf} = 0$ and $\phi = 0$ then the Hamiltonian becomes:

$$H_e = \omega_1 I_x$$

Then there is also:

$$\sigma(\tau_p) = \exp(i\gamma B_1 I_x \tau_p) \sigma(0) \exp(-i\gamma B_1 I_x \tau_p)$$

This makes sense. The magnitude of the rotation will need to be based on the pulse width τ_p and the probe magnetic field B_1 .

If we have raising and lowering operators:

$$I^+ = I_x + iI_y$$

$$I^- = I_x - iI_y$$

We can rewrite I_x as:

$$I_x = \frac{1}{2}(I^+ + I^-)$$

Rotation matrices:

$$R_x(\alpha)I_zR_x^{-1}(\alpha) = I_z \cos \alpha - I_y \sin \alpha$$

For a 180 pulse we'll have $\alpha = \pi$

$$R_x(\pi)I_zR_x^{-1}(\pi) = I_z \cos \pi - I_y \sin \pi = -I_z$$

For a 90 pulse we'll have $\alpha = \frac{\pi}{2}$

$$R_x\left(\frac{\pi}{2}\right)I_zR_x^{-1}\left(\frac{\pi}{2}\right) = I_z \cos \frac{\pi}{2} - I_y \sin \frac{\pi}{2} = -I_y$$

The other rotation matrices are:

$$R_y(\alpha) = \exp\left(i\frac{\alpha}{2}I_y\right)$$

$$R_z(\alpha) = \exp\left(i\frac{\alpha}{2}I_z\right)$$

3.6.1 Multiple Spins

The wavefunctions in the product basis are given by the direct products of wavefunctions for individual spins:

$$\Psi_m = |m_1\rangle \otimes |m_2\rangle \cdots \otimes |m_N\rangle \equiv \prod_{i=1}^N |m_i\rangle \equiv |m_1, m_2, m_3, \dots, m_N\rangle$$

m_i takes all possible values. So there are 2^N wavefunctions for spin- $\frac{1}{2}$ nuclei.

$$A \otimes B = \begin{bmatrix} A_{11} & A_{12} \\ A_{21} & A_{22} \end{bmatrix} \otimes \begin{bmatrix} B_{11} & B_{12} \\ B_{21} & B_{22} \end{bmatrix} = \begin{bmatrix} A_{11}B & A_{12}B \\ A_{21}B & A_{22}B \end{bmatrix}$$

$$= \begin{bmatrix} A_{11}B_{11} & A_{11}B_{12} & A_{12}B_{11} & A_{12}B_{12} \\ A_{11}B_{21} & A_{11}B_{22} & A_{12}B_{21} & A_{12}B_{22} \\ A_{21}B_{11} & A_{21}B_{12} & A_{22}B_{11} & A_{22}B_{12} \\ A_{21}B_{21} & A_{21}B_{22} & A_{22}B_{21} & A_{22}B_{22} \end{bmatrix}$$

The four wavefunctions in the product basis are:

$$|\alpha\alpha\rangle = \begin{bmatrix} 1 \\ 0 \end{bmatrix} \otimes \begin{bmatrix} 1 \\ 0 \end{bmatrix} = \begin{bmatrix} 1 \\ 0 \\ 0 \\ 0 \end{bmatrix}$$

etc.

Angular Momentum Operators

Now we translate our angular momentum operators into the product operator basis. For two spins the translation is

$$I_\nu^{(2 \text{ spin})} = I_\nu^{(1 \text{ spin})} \otimes \mathbf{1} \quad (3.2)$$

where $\mathbf{1}$ is the identity matrix and $\nu = x, y, z$.

For N spins:

$$I_{\nu k}^{(N \text{ spin})} = \mathbf{1}_1 \otimes \mathbf{1}_2 \otimes \cdots \otimes \mathbf{1}_{k-1} \otimes I_{\nu k}^{(1 \text{ spin})} \otimes \mathbf{1}_{k+1} \otimes \cdots \otimes \mathbf{1}_N$$

3.7 The Hamiltonian

We will now use the same matrices that we used to construct the state of a system to construct the interaction of the states.

Here is the most general Hamiltonian.

$$H = H_z + H_J = \sum_{i=1}^N \omega_i I_{iz} + 2\pi \sum_{i=2}^N \sum_{j=1}^{i-1} J_{ij} I_i \cdot I_j$$

For a two spin system, $\mathbf{I}_\nu^{(2 \text{ spin})}$ are the 4x4 operators for the first spin, generated by 3.2 and $\mathbf{S}_\nu^{(2 \text{ spin})}$ are the operators for the second spin. We will drop the superscript.

$$H = H_z + H_J = \omega_I I_z \omega_S S_z + 2\pi J_1 I \cdot S + 2\pi J_2 I \cdot S$$

The J_1 and J_2 are two couplings between the two spins.

state	evolution	observations
ρ	Schroedinger $\dot{\rho} = -i[H, \rho]$	$\text{Tr}(A\rho)$

Figure 3-9: A bit of Quantum

J-Coupling:

$$J_1 = I_z S_z$$

Dipolar:

$$J_2 = I_x S_x$$

3.8 A quick bit of Quantum

If we have a pure state then we can talk about Ψ . In quantum computing any two level quantum system may do:

$$|\Psi\rangle = a|0\rangle + b|1\rangle$$

where a and b are complex.

$$|a|^2 + |b|^2 = 1$$

Then our density matrix ρ would be:

$$\rho = |\Psi\rangle\langle\Psi|$$

In NMR, we really don't see any real pure states. Instead we have to content ourselves by having a density matrix constrained by thermodynamics and the total energy of the system.

$$\text{Tr}(H\rho_B) = E$$

ρ_B is the density of states at the Boltzmann distribution.

The coil will contribute a term in the Hamiltonian. This can perturb the system and change the effective energy levels between two states.

3.9 Hartman-Hahn Condition

The Hartman-Hahn condition is satisfied when:

$$\gamma_I B_I = \gamma_S B_S$$

By examining the terms of the Hartman-Hahn condition we can get an idea of what is going on. γB_0 is proportional to energy. The Hartman-Hahn condition indicates that two spins, I and S have the same energy difference. They are apparently experiencing different magnetic fields, B_I and B_S .

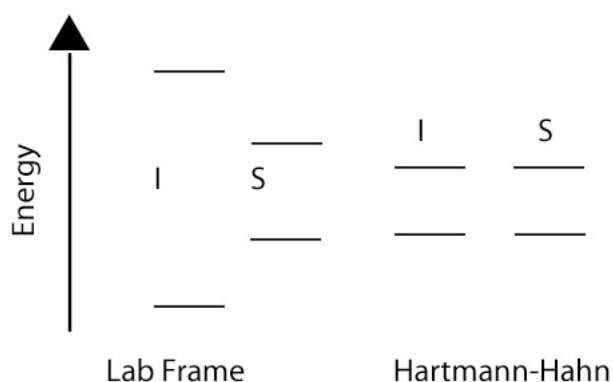


Figure 3-10: Hartman-Hahn Effect - figure produced following Freeman [Fre97].

If the Hartman-Hahn condition is satisfied, then cross-relaxation can occur. If one spin has a larger polarization than the other then some of its polarization will transfer to the latter spin. A theoretical description of Hartman-Hahn can be found in several books [?, CAGPFS96].

3.9.1 ENDOR

Electron Nuclear DOuble Resonance (ENDOR) is a double-resonance technique that utilizes the electron-nuclear dipole hyperfine coupling in spectroscopy.

The Hamiltonian for this system is,

$$H = g\beta\vec{B} \cdot \vec{S} - g_N\beta_N\vec{B} \cdot \vec{I} - \hbar A\vec{S} \cdot \vec{I}$$

where B is the magnetic field, \vec{I} is the nuclear spin and \vec{S} is the electron spin [CP97].

We have only one unit of angular momentum, so only one of two following sets of

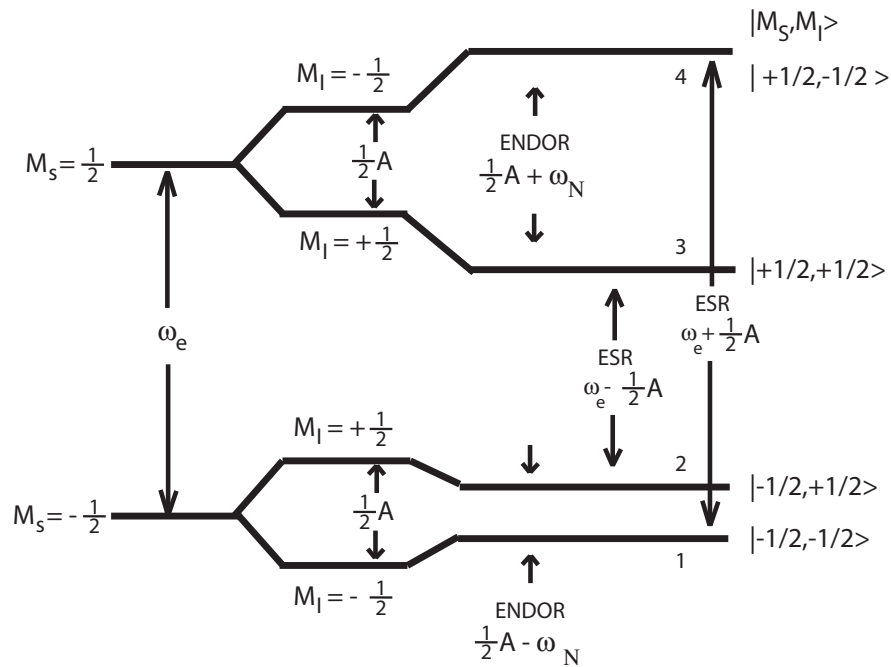


Figure 3-11: Energy level diagram for the $S=\frac{1}{2}$, $I=\frac{1}{2}$. The middle shows hyperfine and the right shows hyperfine and Zeeman splitting. Figure reproduced from [CP97].

transitions is allowed:

$$\Delta M_S = \pm 1$$

and

$$\Delta M_I = 0$$

or

$$\Delta M_S = 0$$

$$\Delta M_I = \pm 1$$

Figure 3-11 shows the energy level diagram for the system described by 3.9.1. It has been assumed that ω_N is less than $\frac{1}{2}A$. This will not be the case in a large magnetic field where the NMR frequency ω_N will be large.

If we observe the ESR spectra at ω_e we will see two lines corresponding to the two allowed transitions, $\omega_e + \frac{1}{2}A$ and $\omega_e - \frac{1}{2}A$. If we put RF in at the $1 \rightarrow 2$ transition, then the ESR peak that corresponds to the $2 \rightarrow 3$ transition will be enhanced relative to the $1 \rightarrow 4$

transition.

The enhancement is limited by the amount of polarization in each state. The NMR frequency is ω_N . If typical polarizations are on the order of 10^{-5} for NMR and around 1000 times larger for ESR, then pumping the $1 \rightarrow 2$ transition will not have a great effect on the ESR spectra. If, however, using the ESR, pump the $1 \rightarrow 4$ transition then there will be significantly fewer nuclear spins available for the $1 \rightarrow 2$ transition compared to the $3 \rightarrow 4$ transition. This difference in spin availability is a polarization enhancement.

3.9.2 INEPT

Insensitive Nucleus Enhancement by Polarization Transfer is a useful pulse sequence for swapping two values of the density matrix. The INEPT sequence is the basis for the SWAP gate in quantum computing. The population is swapped from one spin to another.

3.9.3 COSY and NOESY

CORrelation SpectroscopY and Nuclear Overhauser and Exchange SpectroscopY are two useful spectroscopy techniques.

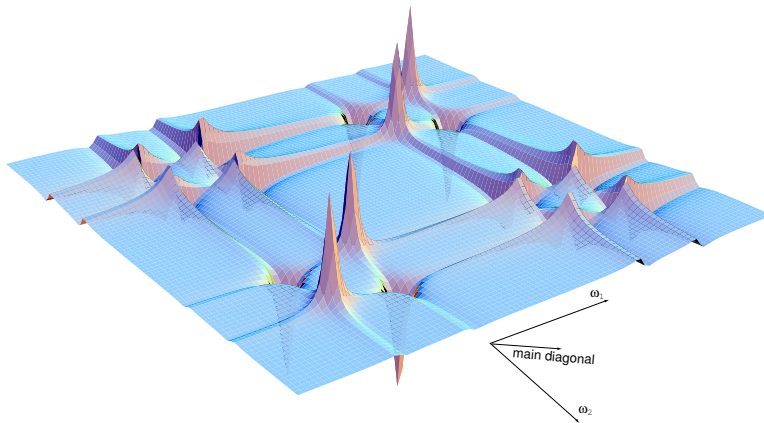


Figure 3-12: COSY spectra. The 1D NMR spectra is along the main diagonal. The off diagonal terms correspond to J-couplings.

Cosy gives us J-coupling chemical shift information. NOESY extracts dipolar coupling. Both require multiple experiments with two pulses where the results are correlated to give a 2D spectra of the spins.

3.10 DNP

Dynamic Nuclear Polarization. For an electron and nucleus that are hyperfine coupled together, we saw in section 3.9.1 that only particular transitions were allowed. DNP ignores that and pumps a transition that causes both

$$\Delta M_S = \pm 1$$

and

$$\Delta M_I = \pm 1.$$

This transition is forbidden to zero order [Jef63], but with sufficient B_1 field, the transition can be accomplished at a rate greater than the relaxation rates of the system.

3.11 CIDNP

Conservation of angular momentum can be the limiting factor in rates of chemical reactions. This is sometimes the case during the observation of Chemically Induced Dynamic Nuclear Polarization (CIDNP) [GB91]. The state of the nuclear spins can affect what products are obtained from a photochemically induced reaction.

Imagine a AB organic molecule. If, "a singlet electronic state is fragmented homolytically in solution to yield to radicals $A\cdot$ and $B\cdot$ " [GB91], that is, if a singlet bond is broken by a photon of the correct energy to disassociate the molecule into two parts, both with an extra unbound electron, then an ISC (inter-system crossing) could be favored. The ISC we're concerned with is the singlet to triplet transition.

As the A part of the molecule moves away from the B part, the energy difference between the singlet and triplet state decreases and the mixing between the singlet $M_S = 0$ state and triplet $M_S = 0$ state can be very sensitive to local magnetic fields. The hyperfine coupling between the electron spin and nuclear spin allow the spin of the nucleus to be a factor in the selection of the singlet or triplet for the reaction product. This assumes that there is a magnetic field around the sample.

For a particular A a spin up proton could prefer the formation of a triplet state while a spin down proton would prefer the formation of a singlet state. The triplet radical pair diffuses away more efficiently than the singlet so the successfully created $A\cdot$ radical would

have a proton spin up polarization. If another C molecule is in solution that combines readily with the radical $A\cdot$ then the observed NMR signal for the AC product would have a polarization towards spin up.

CIDNP is a well established NMR technique. Although this source of increased polarization isn't immediately relevant to this project, an encouraging observation of what *appeared* to be photochemically induced dynamic nuclear polarization in solid-state nuclear magnetic resonance has been reported [ZM96, ZM94]. This increased polarization was observed by shining a Xenon arc lamp on the reaction center sample from a photosynthetic bacteria. CIDNP can be explained by a radical ion pair mechanism, where, while observing a photochemically induced reaction in a liquid, momentum is conserved and as a result of the chemical reaction a perturbation on the nuclear spin is observed. Monitoring of the NMR signal gives information about the photochemical reaction. In this solid-state sample, CIDNP didn't account for the increased polarization. Instead, a recently reported coherent dipolar hyperfine mechanism accounts for the increased nuclear polarization [PM99] observed in this solid-state NMR. The increased polarization was 300 times thermal polarization. The theoretical model that McDermott proposed to explain the increased polarization is not trivial and will require further study to determine it's applicability to our system. This result holds exciting prospects for solid-state NMR of biological molecules.

3.12 MIONP

Microwave-Induced Optical Nuclear Polarization (MIONP) is a DNP technique where a long lived triplet ground state of a molecule is used enhance nuclear spin polarization.

The microwave-induced optical nuclear polarization (MIONP) result for the pentacene polarization experiment [ITS⁺00] suggest that, if we have absorbed angular momentum into a triplet state of a molecule, then we will be able to induce an transfer of angular momentum from the electron spin to the nuclear spin. This will require high power GHz radiation tuned to the triplet nuclear spin splitting.

The key step in this technique is the microwave radiation that pumps the $|0, \frac{1}{2}\rangle \rightarrow |1, -\frac{1}{2}\rangle$ transition. As is common to DNP techniques, we have produced a two spin flip transition. The important attribute of this particular singlet \rightarrow triplet transition is the 12%, 76%, 12% population distribution.

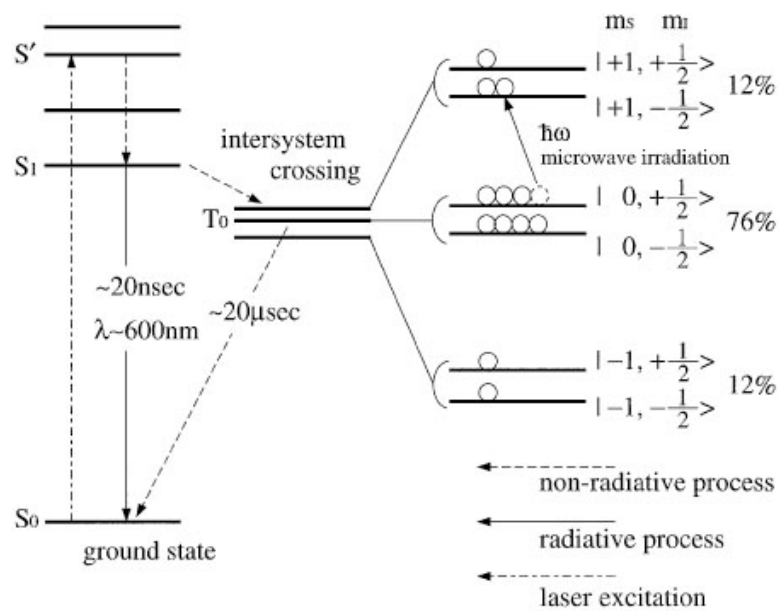


Figure 3-13: The energy levels of Pentacene. Figure from [ITS⁺00]

Chapter 4

Genetic Algorithms

Genetic Algorithms are particularly good at manipulating a large number of variables to look for a solution.

Genetic algorithms (GAs) are computer search algorithms modeled after evolution. Natural evolution has arrived at a number of interesting solutions to maximizing the survivability of a species. GAs take a similar sensibility and apply it to solutions to a problem in a computer algorithm—the algorithm keeps the solutions that work and kills off the rest.

Forrest [For93] has a good review paper in *Science* on GAs. Mathematical modeling books are also good sources for information on GAs [Ger99].

The set of solutions that the computer tries could be said to evolve over time and hopefully converge on a best solution. This evolution is done by duplicating relatively successful solutions and mutating them. The unsuccessful solutions are thrown out.

A search algorithm tries to maximize a fitness function. One could of course try every combination of inputs to a function and fully map out the the output space, but, given finite time, this is usually not the best plan.

GAs are good algorithms to use when the space is fairly flat but has a few regions of great interest. Shaping light to pump an electronic system is well suited for a GA. Most of the shapes will result in no major change in the absorption or emission spectrum but a few pulse shapes can accomplish what Gaussian pulses cannot.

4.1 Algorithm Setup

GAs borrow most of their jargon from biology. The GA is said to *evolve* over time as it converges on a solution. In each *generation* or set of inputs to try, the GA tests each set of inputs, called *genes*, against the fitness function. The fitness function is maximized to find a good solution to the problem. The search is done by *mutating* genes and engaging in gene *crossover* where parts of two genes are combined to arrive at a new set of genes.

A basic implementation of a GA might have 100 genes which consist of strings of 8 bits. These bits could be interpreted as a decimal number and then used as an input to a fitness function. The fitness function could be a mathematical expression or, in our case, an experiment.

The way genes are interpreted is important when considering how to engage in the mutation and crossover steps. During a mutation, parts of the genes are changed randomly. If they are not changed in a reasonable way relative to the bit interpretation then the GA might have convergence problems. For example, if our GA is trying to find the decimal number 255 using an 8 bit binary gene then, if we have a gene with a value of 247, a random flipping of one of the bits will result in one of 246, 245, 243, 255, 231, 215, 183, or 119. For the case of searching for 255, it might be better to do the mutation in base 10 by adding a random number from -10 to 10. This mutation would be better suited to solving the problem.

A gene crossover step has similar hazards. Parameters from two genes can be combined to produce a new gene. It may make sense to group parameters together and call them a *chromosome*. Then when performing a crossover chromosomes may be kept intact.

4.2 Basic Algorithm

Once a way to represent the genes is determined, programming of the GA may begin. First, allocate a set of genes and initialize them to random values. While the GA is running, it iterates in a loop. Figure 4.2 shows the GA flow. First, apply each gene to the fitness function and record the fitness. Sort by fitness then drop bottom 50% or so. Duplicate the best solutions to fill the positions just dropped. Apply mutations and or crossover best suited to the problem. Then repeat.

The details of the implementation of this algorithm is strongly dependent on the prob-

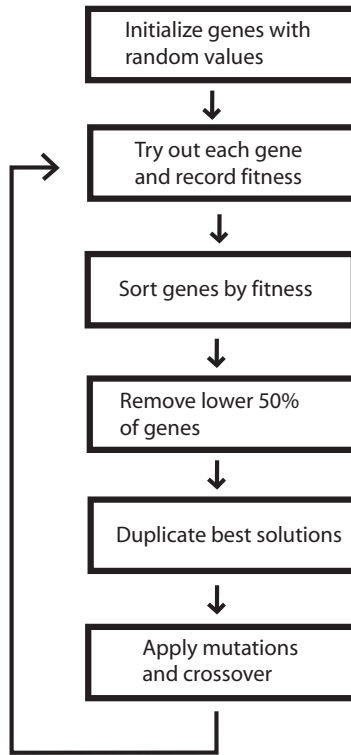


Figure 4-1: GA Flow

lem. A bit of insight into how the the system behaves will generally help convergence. For example, knowing that a particular parameter will have either an exponential or polynomial effect on the resulting fitness, it may be useful to vary that parameter more slowly than another parameter with possibly a lower order effect.

The GA retains a large amount of information from previous generations when creating the next generation. Because of this, the GA should eventually have a set of genes where a few have a good fitness. This may take 20 to 100 generations depending on the type of problem and the parameters used.

When a GA's solutions aren't getting much better as the generations iterate, then the algorithm should be stopped and the results examined. An analytic function that monitors the standard deviation could be used to determine when to halt the GA. It is also likely to be sufficient to just halt the GA after several generations and look at the fitness of the best genes as a function of generation. Figure 4.2 shows the fitness as a function of generation for a GA that didn't converge. Figure 4.2 is for a GA that did converge.

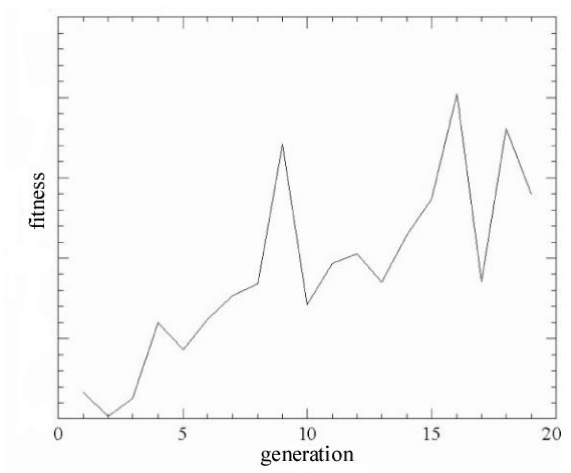


Figure 4-2: This figure shows the progress of a GA running over many generations. The jagged behavior of the fitness indicates a lack of convergence.

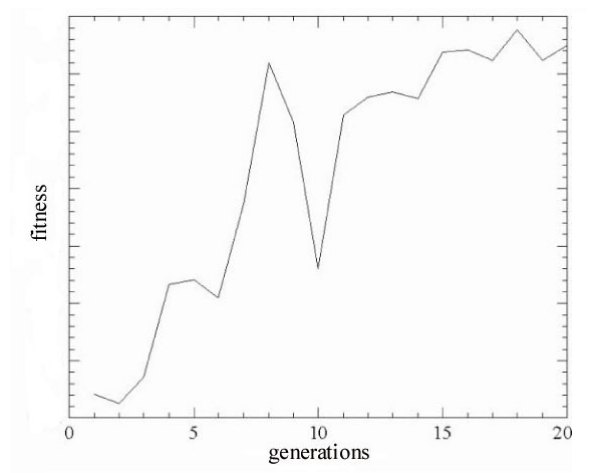


Figure 4-3: This GA seems to have converged on a solution. The smooth behavior over the last few generations is a good indicator of convergence.

Chapter 5

Experimental Exploration

In this chapter we present the story of an experimental exploration of the space related to this thesis. We began knowing that the eventual goal was to increase nuclear spin polarization *some* molecule. In order to monitor nuclear spin polarization, we need a NMR spectrometer. Building one isn't exactly the easiest way to obtain a NMR spectrometer, but the skills gained in the exercise will surely be useful at some point.

The first section of this chapter presents the electronics that were developed that lead to the creation of a few NMR systems. The eventual goal was to integrate one of these NMRs into the Bucksbaum shaped ultrafast laser setup in Michigan. The presentation of these chapters meanders a bit much like the experimental path for the first year.

Towards that goal, we investigated 5 magnets and spectrometers for suitable single shot signal to noise. Section 5.2 reviews each NMR that was investigated for suitability in this experiment. Only two of the magnets available had an existing spectrometer. Spectrometers were made for the rest.

With good specifications for the magnets we can then make a few experimental decisions for the shaped ultrafast pumping experiments. The laser produces only around $1\mu\text{mol}$ of photons. Given typical NMR sensitivities, this is a particularly small number. Section 5.3 reviews the experimental decisions made as a results of this constraint.

5.1 Electronics

Investigation of this thesis required a large amount of hardware development for experimental use. Typically we would design a particular board and send the design files out

for fabrication. The PCB would arrive and then we would solder the boards. Because almost all of these boards were designed for specific frequencies, their specifications generally exceeded those of more general commercial equipment.

Each magnet investigated for suitability has a distinct magnetic field strength and therefore a distinct resonance frequency. Two decades of resonant frequency were covered from 6 MHz to 600 MHz. Most of the hardware developed in this thesis was built with Yael Maguire following the completion of his related Masters thesis [Mag99].

We have made generalized RF boards for signal control, signal generation, and high rate sampling. The hardware is scalable to a large number of channels if necessary for future experiments.

5.1.1 NMR spectrometers

NMR spectrometers have fairly difficult hardware specifications. The recent widespread abuse of fancy walkie-talkies, also known as cell phones, have caused many components used in NMRs to be cheaply available. The noise figures of these devices has improved over the last few years in order to accommodate large amplification needed for long distance wireless signaling.

Figure 3-2 shows a basic NMR spectrometer diagram. An experiment begins with a signal generated by the oscillator and amplified by the lower amplifier in the diagram. The transmit/receive switch in the middle of the diagram allows the signal which is around 30dB to go into the RF coil. The spins in the sample are then tipped over and the switch is sent into receive mode. A signal around -100dB is then sent into the low noise amplifier, then mixed down to near base band, and finally sampled by the computer.

A minimal implementation of a NMR can be seen in figure 5-1. This board has a DDS for signal generation and two switches for transmit/receive. An oscilloscope for data acquisition completes the system. This system was adequate for finding an NMR signal, but the signal to noise performance wasn't adequate for chemical identification. The probe, figure 5-2, is a simple singly resonant RLC circuit. The sample tube has a standard NMR tube diameter of 5mm.

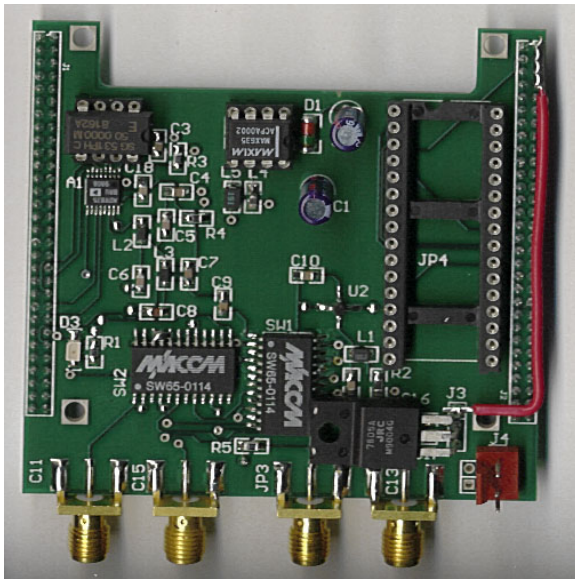


Figure 5-1: mini NMR board

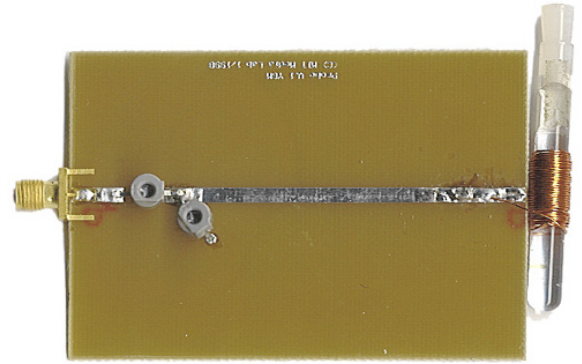


Figure 5-2: minimal NMR probe

5.1.2 FPGAs and Verilog

I thoroughly enjoyed picking up Verilog. The system shown in Figure 5-3 is a complete implementation of a NMR spectrometer. The controller board used a Field Programmable Gate Array (FPGA) to drive the data acquisition board and the signal generator.

The FPGA is effectively a re-programmable Application-Specific Integrated Circuits (ASIC). The programming language we used is called Verilog. A Xilinx XCS30XL FPGA was used in three of the NMR boards. The Verilog compiler allows for specific timing constraints. In general this is an important factor when using a NMR.

Verilog as a programming language looks pretty similar to C. The main difference between Verilog and C is that Verilog executes all statements in a block simultaneously. This means that sequential operations must be clocked in a separate loop. The FPGA is very parallel. Two clocks without a common source can be running on the same FPGA at the same time. This is particularly useful since the alternative to a FPGA is to use off the shelf chips. These are usually fine, but the sequential programming model does not easily lend itself to RF phase control.

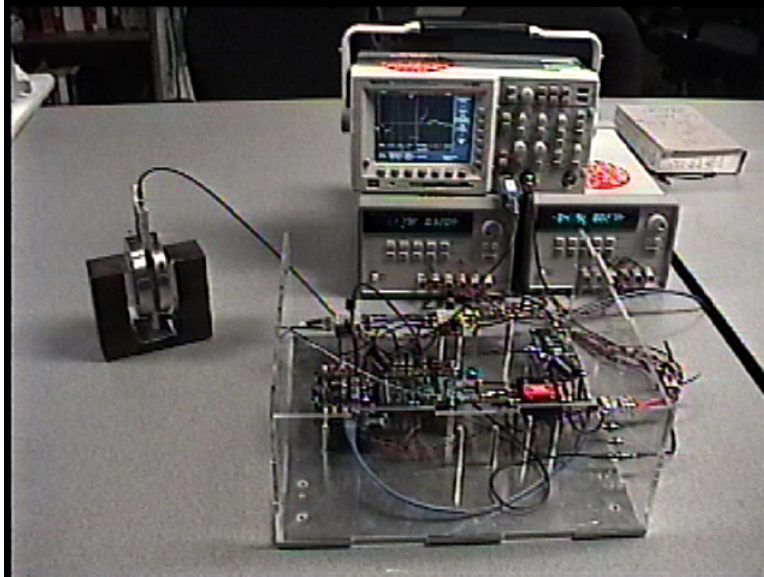


Figure 5-3: Complete Tabletop NMR System

5.1.3 Boards

The final versions of the NMR spectrometer electronics were controlled by Pengachu¹ μ Linux² boards.

The heart of the spectrometer is the controller. The Pengachu project (Figure 5-4) was responsible for the in-house development of this controller. The backplane communication is 1 Mbps SPI. A 10 Mbit ethernet controller is on the board along with a serial port.

We run μ Linux on the Motorola Dragonball processors.

Figure 5-5 shows an analog receive board. There is a 80 db of gain on the front end followed by a mixer and finally a small bit of gain as the signal leaves the board to be digitized later in the flow.

Figure 5-6 shows the PCB for the signal generation board. A fixed frequency DDS and programmable waveform generator were used. Figure 5-7 shows a Pengachu linux box mated to an acquisition board. The boards were all stackable.

¹Developed by Matt Reynolds, Rehmi Post, and Wendy Ju at the MIT Media Lab

²Embedded Linux/Microcontroller open source project. <http://www.uclinux.org/>

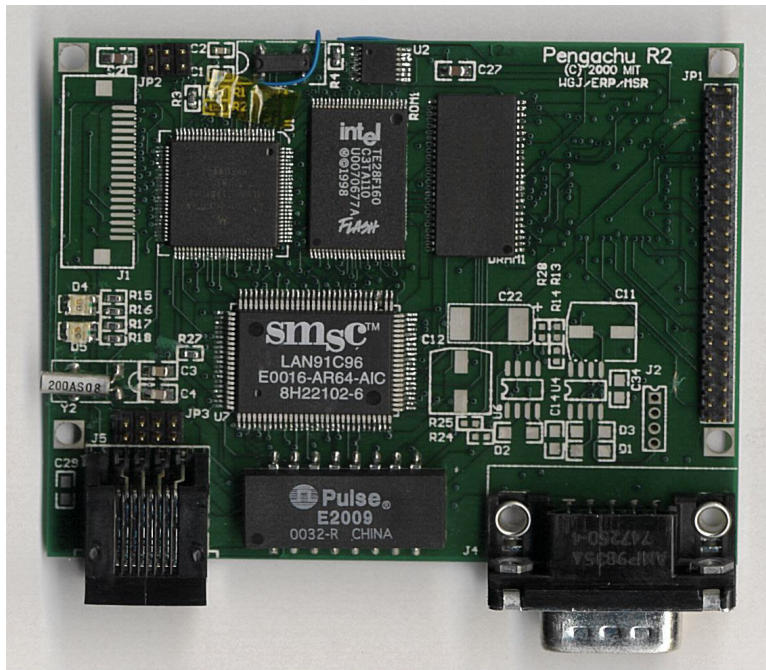


Figure 5-4: Pengachu Linux Box

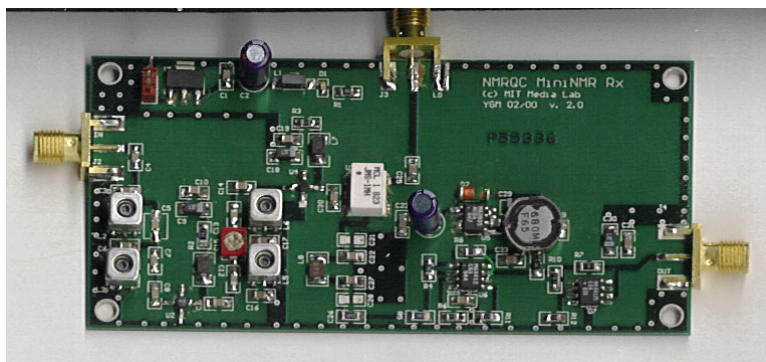


Figure 5-5: Analog RX Board

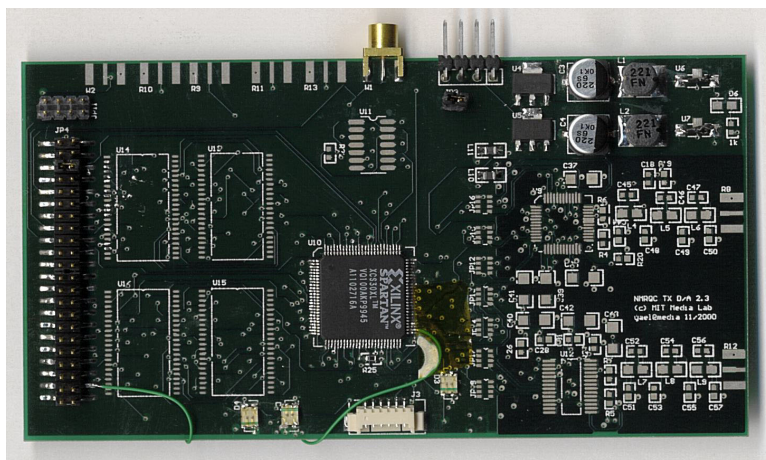


Figure 5-6: Signal Generation board

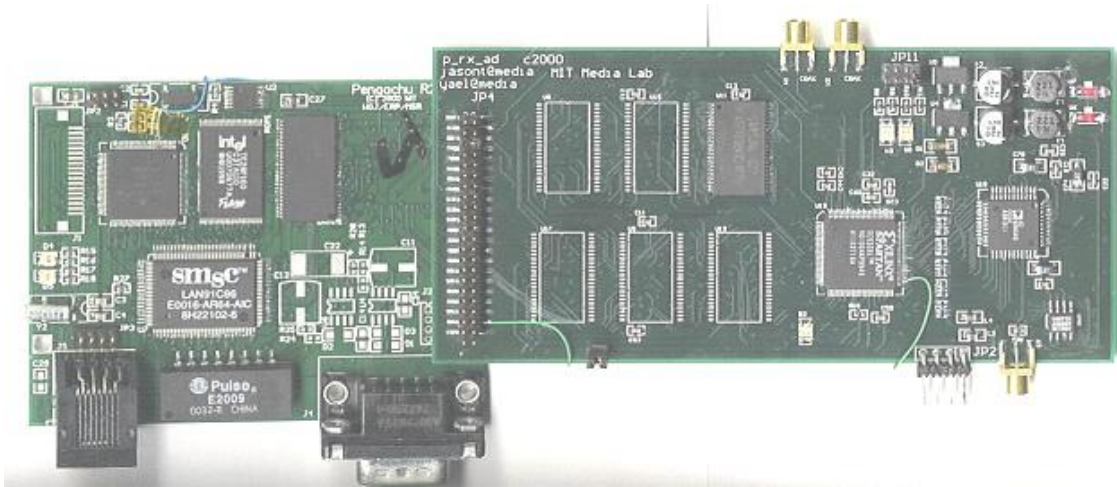


Figure 5-7: Pengachu with data acquisition board

5.2 NMR Systems

As reviewed in Chapter 4 Genetic Algorithms require a large number of trials while searching for a solution. Each trial in our case is a separate NMR experiment. This implies that we will not have a long time to average so the signal to noise is important.

Five magnets were examined for suitability in this experiment. In order to characterize a magnetic field for use in a NMR, the only reliable way is to find an NMR signal in the system. This required development or purchase of spectrometer electronics for each magnet.

The 500MHz Varian magnet came with a spectrometer. The other four spectrometers were developed in house. Development of NMR spectrometers is covered in the Chapter 5.1 of this thesis. A more extensive description can be found in a masters thesis by Yael Maguire [Mag99].

We need to pump a sample with only 1 μmol of photons and still have some transmitted light to use for feedback. This means that our sample density to be comparable to the number of photons (see Chapter 5.3).

This constraint makes the signal to noise ratio (SNR) of a complete NMR spectrometer the most important metric. In the case of these magnets, the physical size of the magnet trended with the SNR. Unfortunately, these magnets were located in Cambridge, MA, and our collaborators with the laser in the Bucksbaum group were in Anne Arbor, MI. This separation introduced a size constraint causing us to focus on portable magnets.

Single-shot SNRs of the magnets respective spectrometers are recorded in chapter 5.3. Signal-shot SNR, without averaging, is important because the GA used in a feedback experiment must be able to evaluate each gene quickly. A GA run must be completed within an hour or two.

5.2.1 Table top magnet

We³ developed the final embodiment of the Table Top NMR project that has been carried by various⁴ students in Neil Gershenfeld's Physics and Media group at MIT.

Figure 5-8 is a singly resonant probe tuned to 8 MHz. The sample tube is 5mm in diameter. For the SNR measurements we used glycerine for our NMR sample. The magnet

³Yael Maguire and Jason Taylor

⁴Rich Fletcher, Matt Reynolds, Yael Maguire and Henry Chong

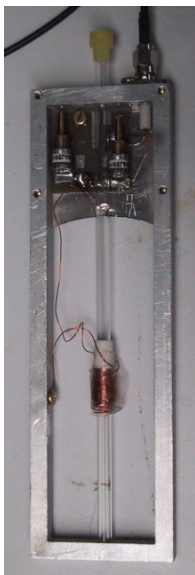


Figure 5-8: Table top magnet probe tuned to 8 MHz



Figure 5-9: Table top magnet: 0.18 T field

in figure 5-9 is approximately 10 inches tall. This magnet was originally designed by Yael Maguire for use in his masters thesis. His intended to make the magnet as portable as possible.

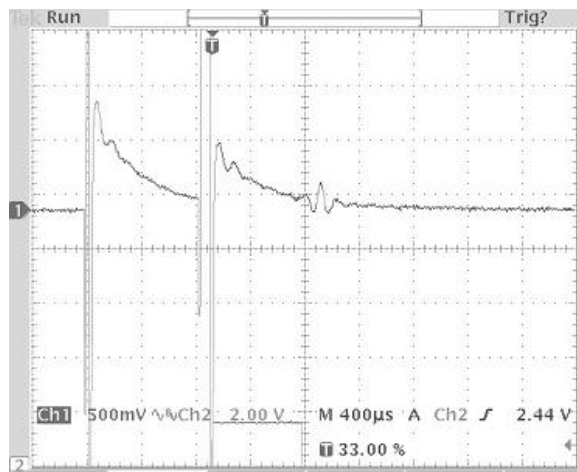


Figure 5-10: NMR Spin Echo trace from table top magnet

We were able to find an NMR signal from the table top magnet. The signal to noise for that spectrometer and magnet was around five. The field was measured to be 0.187 Tesla.



Figure 5-11: Halbach cylinder probe; created by Isaac Chuang

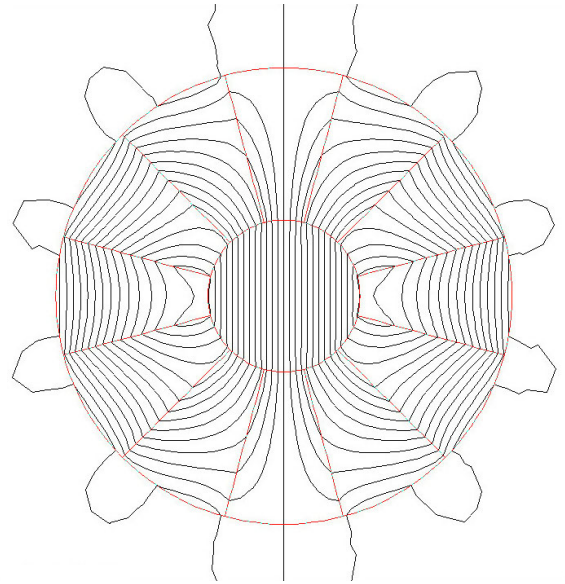


Figure 5-12: Halbach field lines [Mag99]

5.2.2 Halbach Cylinder NMR

The Halbach cylinder is made by modeling the fields of a dipole and then making a set of permanent magnets with the same field directions. When assembled properly the magnetic field is uniform inside the bore of the magnet. The magnet we used was produced by Magnetic Solutions, a company located in Ireland that was founded at Trinity College in Dublin.

This Halbach cylinder magnet (figure 5-17) is made from 12 segments assembled in an aluminum can. The field is perpendicular to the bore of the magnet. A theoretical treatment of the magnetic fields can be found in chapter 7.3 of Maguire [Mag99]. Figure 5-12 shows the field lines for a Halbach cylinder.

The laser must come in parallel to the magnetic field. This presented a slight problem when considering the Halbach cylinder design. To address this problem two mirrors were mounted on shafts on either side of the sample at 45 degrees. This would allow light to come

in from below the sample bounce through the sample and return back down. Figure 5-13 shows the final version of the sample holder and mirrors.



Figure 5-13: Sample holder with mirrors; Design and construction by Daniel Benhammou, MIT

Ultimately we were unable to find an NMR signal on this magnet. The homogeneity of the field was not sufficient for the NMR signal to be detectable by even the best of our spectrometers. Upon profiling the magnetic field, the inhomogeneity across a standard sample size was determined to be poor enough to cause a frequency spread of 21 kHz. This broad frequency spread causes the power of the NMR signal from the spins to be too weak for detection.

After finding no NMR signal and subsequently determining that the field homogeneity was insufficient. We decided that no NMR signal was likely to be found, so SNR was recorded as zero.

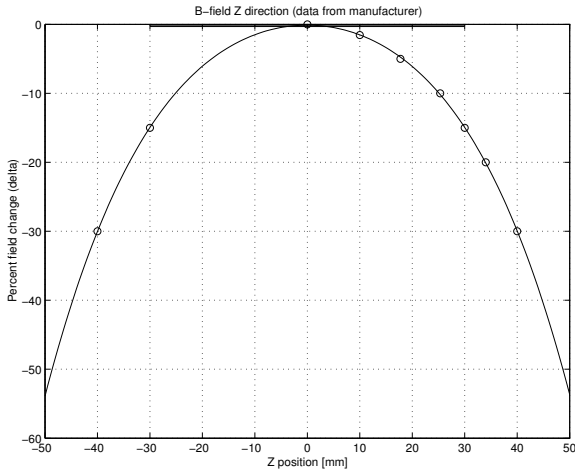


Figure 5-14: Z field homogeneity according to manufacturer specs. The inhomogeneity across 3.730 mm is at best 22.607 kHz.

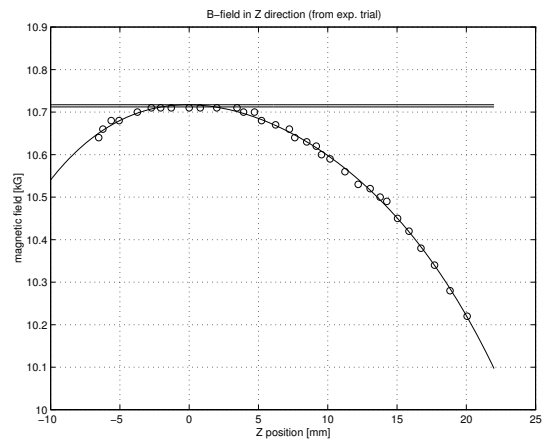


Figure 5-15: Z field homogeneity measured in lab. The inhomogeneity across 3.730 mm is at best 21.728 kHz.

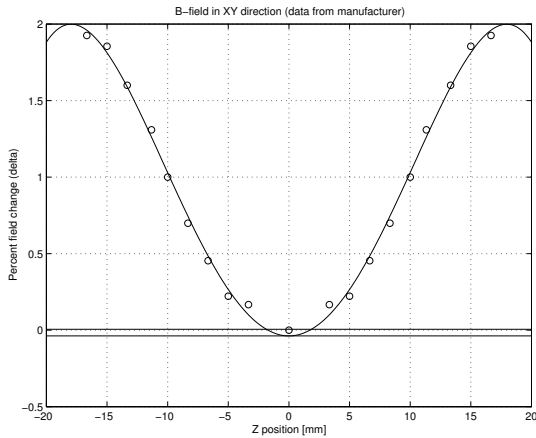


Figure 5-16: XY field homogeneity according to manufacturer specs. The inhomogeneity across 3.730 mm is at best 19.717 kHz.

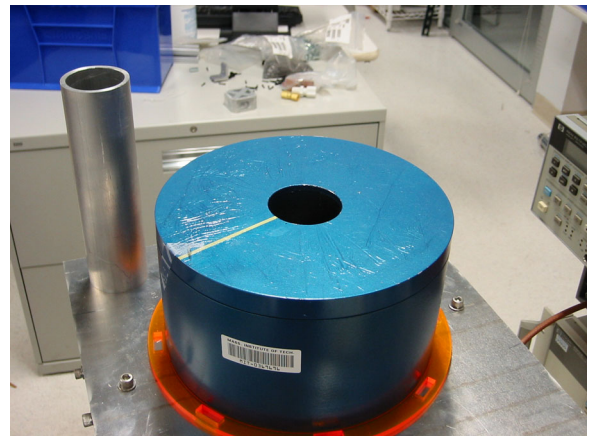


Figure 5-17: Halbach cylinder magnet

5.2.3 Electromagnet

The electromagnet has a variable field and adjustable spacing between pole pieces. The electromagnet was purchased from GMW Associates. The field can be adjusted up to a maximum of 1.6 Tesla. The field homogeneity was 1ppm over a 0.5cm diameter sphere.

The magnet power supply requires water cooling. During Yael's tenure [Mag99] the magnet was installed. A heat-exchanger is required for operation as well as three-phase power.



Figure 5-18: Electromagnet magnet.

The variable field of this magnet made it an attractive candidate for many potential experiments. We have considered creating an ESR spectrometer. The electron spin resonance is around 28 GHz/Tesla. At both 28 GHz and 14 GHz standard commercial RF equipment is available that would make development of the spectrometer considerably easier. A sample holder with mirrors would have to be designed, as shown in Figure 5-13.

The signal to noise of the electromagnet was around 50. This sufficed for experimental equipment development, but it is unlikely to be sufficient for any experiment that we may do with Professor Bucksbaum's group.



Figure 5-19: 200MHz superconductor magnet with Jason for scale



Figure 5-20: 500MHz superconductor magnet with Jason for scale

5.2.4 500 MHz and 200 MHz Superconducting Magnet

Commercial superconductor magnets are available in the 200 MHz to 800 MHz range. The frequency rating indicates the Hydrogen resonance frequency in the field. Hydrogen resonates at 42.58 MHz/Tesla.

The 500 MHz spectrometer is used in quantum computing experiments in Isaac Chuang's lab and the 200 MHz spectrometer was used for equipment development in Neil Gerhsenfeld's lab. The 500 MHz magnet has a magnetic field of 10.5 Tesla.

Several samples have been run on both NMRs. These magnets are solenoid in design so the magnetic field is parallel to the bore of the magnet. This geometry will be particularly useful when it comes time to pump a NMR sample inside the bore of the magnet.

The 500MHz signal to noise was determined to be around 20,000. The SNR of the 200MHz magnet was around 1000.

5.3 1 μmol of Photons

Given the space of all molecules in liquid, solid, and gas phases we had to make some decisions. The number of photons was the main design constraint.

5.3.1 Photon Budget

A firm constraint in this thesis is the number of photons compared to NMR polarization. NMR polarizes relatively few nuclei in a sample. Typical polarizations are $O(10^{-5})$. For this experiment each pulse can be as high as 2 mJ of energy at 800 nm photons.

$$\frac{2\text{mJ}}{1.602 \times 10^{-19}\text{J/eV}} = 1.248 \times 10^{16}\text{eV}$$

$$\frac{1240 \text{ eV} \cdot \text{nm}}{800 \text{ nm}} = 1.55 \text{ eV} \rightarrow 8.05 \times 10^{15} \text{ photons}$$

At 10 Hz we have around 1 μmol of photons.

When in an all-optical experiment, the GA runs at a rate of around 10 gene evaluations per second. Eventually we would like to integrate a NMR into the feedback fitness function. In order to for that to happen, the rate at which data is gathered via the NMR can't be too much worse than the all-optical rate.

5.3.2 Magnets

To determine what magnet was required for this project, we experimental signal to noise ratios for each magnet.

magnet	field (T)	SNR	diameter	cost
small permanent	0.1	5	0.5 feet	\$2k
halbach cylinder	1	0 (no signal)	1 foot	\$8k
electromagnet	0.5	50	3 feet	\$40k
200 MHz super-con	4.7	1000	2.2 feet	\$30k
200 MHz super-con R2D2	4.7	1000	2 feet	\$30k
500 MHz super-con	11.7	20000	3.5 feet	\$200k

The signal to noise ratio (SNR) goes as the field raised to the 9/5's power [Mag99].

$$\text{SNR} \propto B^{\frac{9}{5}}$$

The following table illustrates the importance of field strength to signal to noise. This table will just give us a first guess as to the relative SNRs. The electronic front end will determine the rest of the SNR.

magnet	field (T)	9/5's SNR guess
small permanent	0.1	0.0552
halbach cylinder	1	3.4822
electromagnet	0.5	1 (normalized to this)
200 MHz super-con	4.7	56.4
200 MHz super-con R2D2	4.7	56.4
500 MHz super-con	11.7	291

All of these signal to noises are experimental values for Hydrogen in either a glucose or water sample.

We need to be able to detect a polarization change which corresponds to 1 μmol (6.02×10^{17}) of additionally polarized nuclei.

5.3.3 Boltzmann Sample Polarization

A quick calculation gives a good number to keep in mind for the number of nuclei polarized by our magnet.

Water density is 1 g/mL. Our sample volume is

$$\pi \times (2.5\text{mm})^2 \times 10\text{mm} = 194.6\text{mm}^3 = 0.194\text{cm}^3$$

$$194\text{mm}^3 \equiv 0.194\text{mL} \equiv 0.194\text{g}.$$

Water is $18 \frac{\text{g}}{\text{mol}}$ (amu).

$$0.194\text{g of water} \equiv 0.0108\text{mol} \equiv 10811\mu\text{mol}.$$

Typical NMR sample polarization is 10^{-5} . So how many nuclei will be polarized by the magnet?

$$10811\mu\text{mol (in the sample)} \rightarrow 0.108\mu\text{mol (polarized by the magnet)}$$

5.3.4 Coumarin 500 ($C_{12}H_{10}NO_2F_3$)

The laser dye used in our optical pumping experiments was Coumarin 500 ($C_{12}H_{10}NO_2F_3$). Figure 5-21 is a ball and stick diagram of Coumarin 500. The atoms are all clearly labeled in the figure. The small dots near the Fluorines are lone pairs.

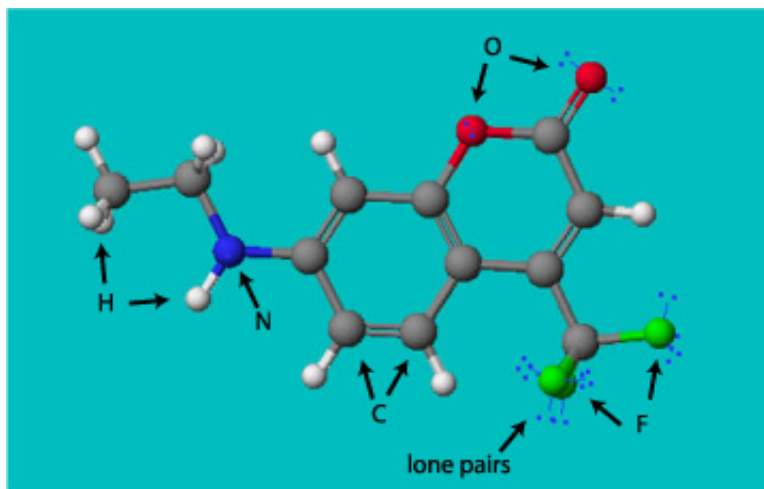


Figure 5-21: Coumarin 500

We know that the $1s$ orbital of Carbon is fully populated with electrons. This means that the valence electrons that may be involved in bonding will be from the p orbital. The Carbon-Carbon bonds are all either double π bonds or single π bonds as indicated by the number of lines connecting the two atoms. All of the bonds with Hydrogen are σ bonds the rest are π bonds.

We chose Coumarin 500 for a few reasons. The transition from a singlet to a triplet state in Coumarin is known. The three Fluorines initially were attractive. Early in preparing for this experiment, we believed that a small or possibly table top magnet would be sufficient for this NMR experiment. The NMR Fluorine spectra would have no solvent peaks since the solvents we were use, methanol and ethanol contain no Fluorine.

Notice the absorption peak in Figures 5-22 and 5-23. In this experiment we pump the 400 nm absorption line.

Optical Density

Remember the Beer-Lambert Law

$$A = \epsilon bc$$

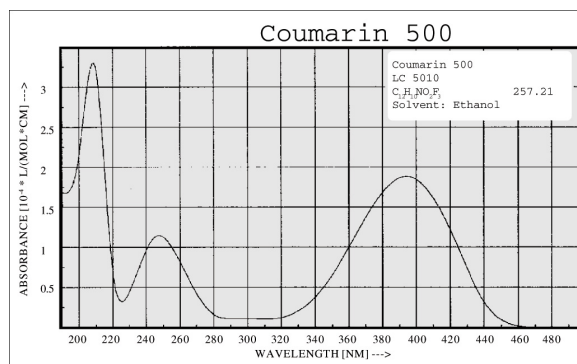


Figure 5-22: Coumarin 500 UV-VIS; reproduced from [LP02]

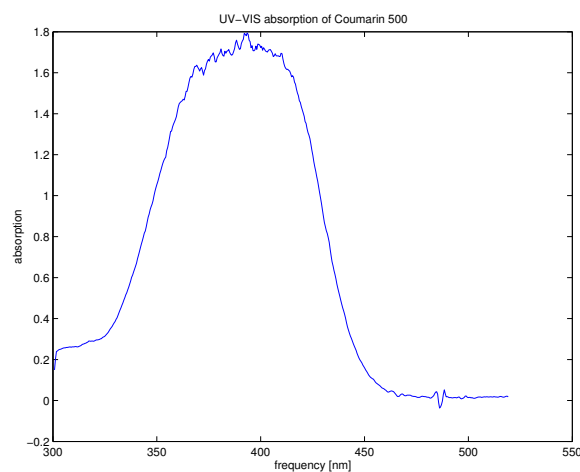


Figure 5-23: UV-VIS Data of Coumarin 500

$A = \text{absorbance} \rightarrow A = \log_{10} P_0/P$; where P/P_0 is the transmittance

$b = \text{path length}$

$c = \text{concentration}$

$\epsilon = \text{molar absorptivity}$

We will try 0.1% transmittance for an absorbance of 1.

Coumarin 500 properties:

MW = 257.21

abs max = 395nm

$\epsilon = 1.85 \times 10^4 \text{ L mol}^{-1} \text{ cm}^{-1}$

$b = 1 \text{ cm} = \text{optical path length}$

$a = 1$

$$c = \frac{1}{b\epsilon} = \frac{1}{1\text{cm} \cdot 1.85 \times 10^4 \text{L/mol/cm}} = 0.0000541 \frac{\text{mol}}{\text{L}} = 541 \frac{\mu\text{mol}}{\text{L}} = 0.541 \frac{\mu\text{mol}}{\text{mL}}$$

how many moles for a sample volume of 0.194mL?

$$0.541 \frac{\mu\text{mol}}{\text{mL}} * 0.194\text{mL} = 0.105\mu\text{mol Coumarin 500}$$

We should compare this molar density to water in order to determine our expected signal to noise for each magnet.

In water we have 10811 μmol of H₂O or 21622 μmol of H. In this sample we'll have 10 Hydrogens per Coumarin 500 so this is so we're looking at about 1.05 μmol of H.

Thus a *rough* guess at the signal to noise ratio needed is:

$$\frac{H_{\text{water}}}{H_{\text{coumarin 500}}} \approx 10,000.$$

If we assume that the concentration could be greater by a factor of 10, then the SNR will be in the approximate range for a small superconductor magnet.

5.3.5 NMR of Flourine

We⁵ ran three Flourine spectras on a 500MHz NMR.⁶

sample	concentration	F signal	SNR
Freon (CCl ₃ F)	80%	2.9397e9	27418
Coumarin 500 in MeOH	0.020g/10mL (low)	8.1592e6	27
Coumarin 500 in MeOH	0.219g/10mL (saturated)	5.2412e7	317
Coumarin 500 in MeOH	0.005g/10mL (lowest)		≈10

If we compare the atomic concentrations we can obtain estimated signal strength in each magnet. For the high concentration Coumarin sample we'll use 0.100g/10mL rather than 0.219g/10mL since the sample had undissolved Coumarin in the bottom of the flask. This 0.100g/10mL concentration was gotten by comparing the Fluorine peaks in the NMR runs.

⁵Special thanks to Matthias Steffen for NMR help.

⁶saturated means that there was solid undissolved dye in the bottom. Actual dissolved amount was probably around 0.1g/10mL

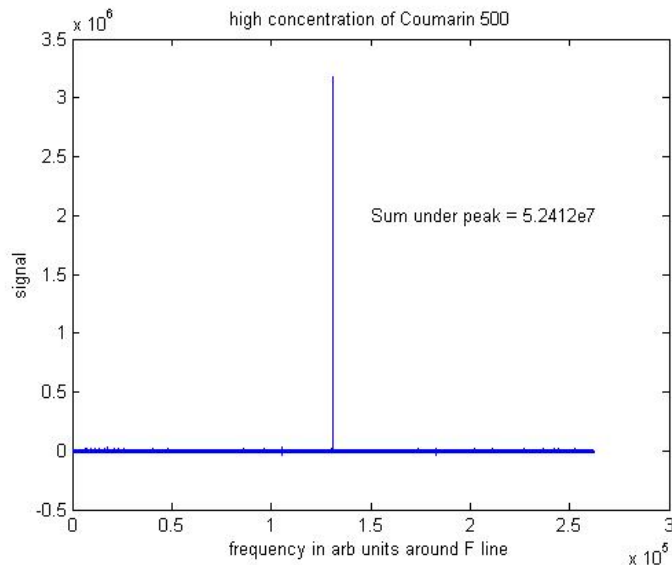


Figure 5-24: high concentration coumarin 500 nmr sample: F

sample	molar concentration	H density	F density
Freon (CCl ₃ F)	5830.90 $\mu\text{mol/mL}$	0	5830.90 $\mu\text{mol/mL}$
Coumarin 500 (low)	7.78 $\mu\text{mol/mL}$	77.78 $\mu\text{mol/mL}$	23.34 $\mu\text{mol/mL}$
Coumarin 500 (high)	38.9 $\mu\text{mol/mL}$	389 $\mu\text{mol/mL}$	116.7 $\mu\text{mol/mL}$

The Fluorine signals from the NMR are roughly proportional to the densities. The NMR signal ratios are 1:6 and 1:360 for low:high and low:Freon respectively.

The high:Freon NMR signal ratio is 56.

It looks like the supercon magnets have sufficient signal to noise. We'll have about 5 bits of resolution on that signal.

5.3.6 Hydrogen might be better

After simulating the electronic system in CAChe (see appendix 1) it looks likely that the Fluorine nuclei isn't the best choice. There is no activity around the Fluorine atoms with 400nm light. The hydrogen signal should work well since there are hydrogens all around.

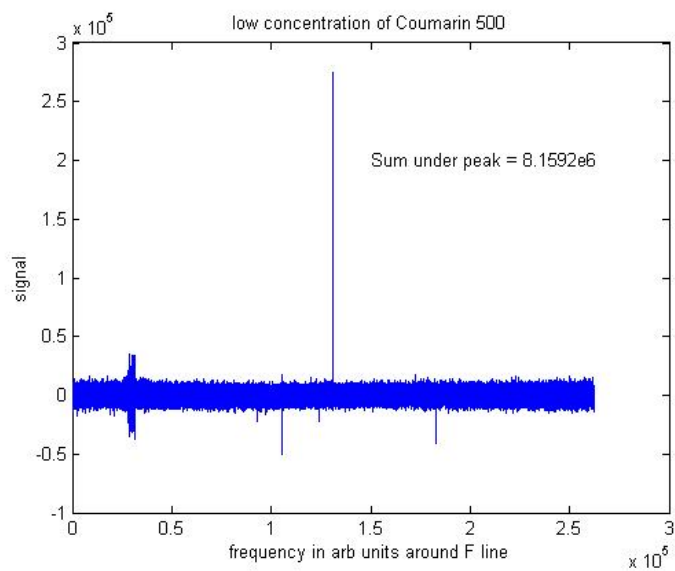


Figure 5-25: low concentration coumarin 500 nmr sample: F

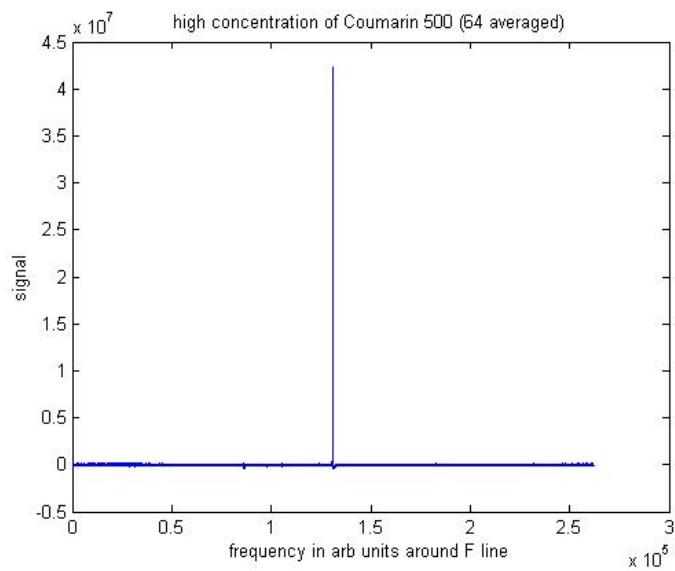


Figure 5-26: high concentration coumarin 500 nmr sample: F; avg 64

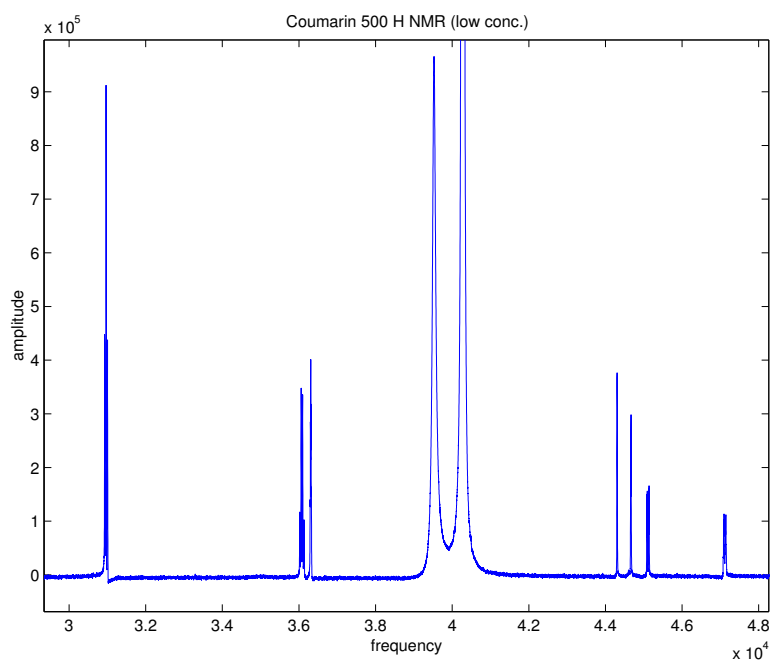


Figure 5-27: low concentration Coumarin 500 NMR sample: Hydrogen

Chapter 6

Proposal for Experiments

This Chapter presents a proposal for experiments designed to investigate the utility of shaping ultrafast pulses for improving polarization in NMR systems. In the preceding we Chapters presented a pedagogical review of the relevant fields and related experimental work.

Laser dye molecules are used to make dye lasers. The singlet* \rightarrow singlet transition is preferable for laser efficiency. A small percentage (1-3%) of the time a singlet* \rightarrow triplet transition might occur. In the triplet state, the angular momentum is in the spin configuration of two electrons.

Our sample is Coumarin 500—a laser dye. We would like to use a shaped ultrafast pulse to increase the transition to the triplet state and then, if necessary, use microwave radiation to move the spin angular momentum of the electron to the nuclear spin.

Given the tremendous success of optical pumping in the gas phase and the encouraging results of increased polarization in other systems as seen in Chapter 3, we expect that a novel pulse shape of circularly polarized light from an ultrafast laser will allow us to transfer angular momentum into the molecule and eventually the nuclear spin.

A pulse shape chosen to increase polarization will be searched for by a Genetic Algorithm (GA) learning algorithm. Because of the complexity of the electron angular momentum, electron spin, and nuclear spin interaction, we approach this process in several steps.

6.1 Maximize Absorption of Angular Momentum

Shaped ultrafast pulses have been successfully used to control quantum dynamics of molecular systems.

We would like to show that shaping the pump beam of circularly-polarized light is able to increase the amount of absorbed angular momentum. The GA should be able to do something towards accomplishing this task. The absorption of angular momentum is a necessary first step towards obtaining high nuclear spin polarization.

We present the experimental pump probe setup as well as some preliminary results in Chapter 7.

6.2 Nuclear Spin Polarization

If we have a pulse shape that causes increased absorption of angular momentum in the molecule then there is a possibility that we have increased nuclear polarization.

It is conceivable that if we were able to absorb a great deal of angular momentum into our molecule, then via an electron-nuclear spin hyperfine coupling we may see increased nuclear polarization from only shaped optical pumping.

We will use a NMR spectrometer with a probe designed to accept a laser pulse to detect a change in nuclear polarization. Due to the low sample concentration a high resolution NMR will be required for this step. In Chapter 5 we discuss the signal to noise requirements.

The next step will be to monitor nuclear spin polarization. If we have a pulse shape that causes increased absorption of angular momentum in the molecule there is a possibility that we have increased nuclear polarization.

Monitoring nuclear spin polarization of a sample in-Situ with transmitted laser light will be very difficult. Due to the low sample concentration a high resolution NMR will be required for this step. In Chapter 5 we discussed the signal to noise requirements.

A 600 MHz magnet has been installed in a lab down the hall from the laser used in the previous experiment. Based on our measurements with the 500 MHz NMR at MIT, the 600 MHz magnet should provide adequate polarization to observe a sample with an optical density of one.

In this experiment, the procedure will be basically the same, except, in addition to watching the transmission of light, we will be monitoring nuclear spin polarization. We



Figure 6-1: 600 MHz Magnet at the University of Michigan

may also include the nuclear polarization measurement in the fitness function for the GA.

6.2.1 Light vs. Dark NMR signal

The initial experiment will be done with only the pump beam going into the sample. First we will find a good pump shape outside the magnet and then send just the pump into the NMR and look for a change in polarization. If a difference between the NMR spectrum with the light on versus the spectrum with the light off, then we will be able to use the NMR signal to adjust the pulse shape.

A 600 MHz NMR probe will have to be modified to allow light to pass through the sample.

6.3 Electron Spin Angular vs Orbital Angular Momentum

When we put in $h\nu$ of energy and \hbar angular momentum we know that for this molecule the energy generally goes into a singlet to excited-singlet transition. This corresponds to the angular momentum going into orbital angular momentum. From there, the electron could radiatively relax down to the ground state. The electron could also make a [singlet₁ \rightarrow triplet₀] transition where 1 unit of angular momentum arrives in the S electron spin configuration.

By just looking for absorption of angular momentum we will not be able to tell the difference between these two processes.

6.3.1 Phosphorescence

A good intermediary experiment might be to select a molecule with a known phosphorescence transition from the triplet state back down to the singlet state. If we monitor the phosphorescence via a fluorescence up-conversion experiment where the gate is placed some time after the fluorescence is finished and before the phosphorescence signal is gone. Then using this signal in our fitness function will allow us to directly measure the singlet to triplet ISC rate. It seems highly likely that a shaped ultrafast pulse would be able to maximize that transition. This experiment would have to be called a phosphorescence up-conversion experiment.

6.4 Electron Polarization Transfer to Nuclear Spin

If we establish large polarization in the electron state, if only for $20\mu\text{s}$ or so, we should be able to transfer the polarization via an MIONP transition saturation technique, or possibly ENDOR.

The microwave-induced optical nuclear polarization (MIONP) result for the pentacene polarization experiment suggest that, if we have absorbed angular momentum into a triplet state of a molecule, then we will be able to induce an transfer of angular momentum from the electron spin to the nuclear spin. This will require GHz radiation tuned to the triplet nuclear spin splitting.

In experiments like the Microwave-Induced Optical Nuclear Polarization (MIONP) discussed in Chapter 3, the polarization is built up over several hours. If we attempt a

microwave-induced polarization transfer, the state of our experimental equipment will affect how we proceed. The 600 MHz NMR spectrometer is not yet operational so we cannot get a signal to noise value. In a 14 Tesla field, the ESR spectra will be around 390 GHz. An ESR spectrometer at that frequency will require a large time commitment in experimental development. It is possible that we may first opt for a more modest experiment in an optically dense sample. The increased sample concentration would reduce the need for a large magnetic field and a 0.5 Tesla spectrometer with a 14 GHz ESR spectrometer should be easier to setup.

Chapter 7

Preliminary Results

7.1 Absorption of Angular Momentum

Preliminary results were obtained through a collaboration between Phil Bucksbaum's group at the University of Michigan and Neil Gershenfeld's group at MIT. All NMR data was collected at MIT and all of the optical experiments were done at U. Michigan.

Here we present the setup of the all-optical experiment and discuss future experimental details.

7.1.1 The Laser

This specific laser setup has been used in experiments in the past. The following paragraph is taken from a review article by Bucksbaum et. al. [PWWB01]:

The control light field is made with a Kerr lens mode-locked (KLM) titanium sapphire laser that produces 100 fs pulses with about 5 nJ of energy at a central wavelength of 790 nm. The pulses are temporally dispersed to 150 ps in a single grating expander and amplified to 2 mJ in a regenerative amplifier at 10 Hz. The output of the amplifier is split to form two beams. One beam is sent to the pulse shaper, and the other is used as an unshaped reference for spectral interferometry measurements of the shaped pulses. The pulse shaper consists of a zero dispersion stretcher with an acousto-optic modulator (AOM) in the Fourier plane, where different colors in the light pulse map to different positions on the modulator. The AOM carries a shaped acoustic traveling wave, which

diffracts different colors with different phases and amplitudes. These colors are reassembled at the output of the pulse shaper, yielding a temporally shaped laser pulse. In order to compensate for the low efficiency of the pulse shaper (10 - 15%), we reamplify the shaped pulses in a low-gain multipass amplifier. The pulses are then compressed in a single grating compressor. The resulting shaped laser pulses are then directed into the molecular sample to be studied, and a predetermined feedback signal is monitored.

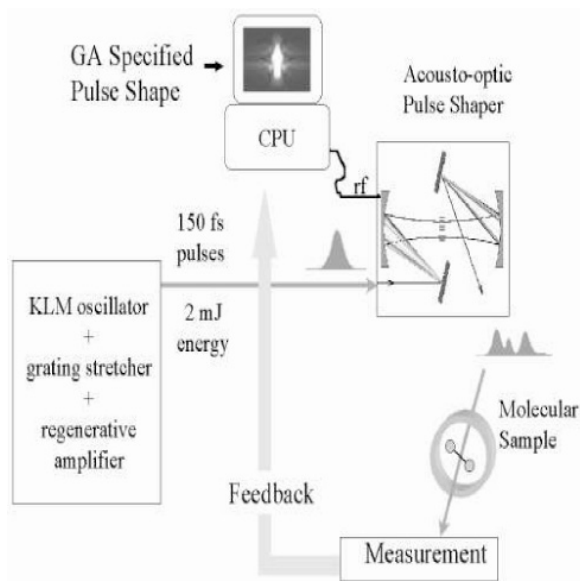


Figure 7-1: Ultrafast Laser with AOM diagram from [PWWB01]

7.1.2 The GA

Genetic algorithms have proven to be effective in finding novel pulse sequences [BDNG01, PWWB01].

The Genetic Algorithm involved in this research controlled the parameters on the acousto-optic modulator (AOM) controls the shape of the light. The shaping is done by putting the light into a zero order dispersion stretcher and using the AOM, in the Fourier plane of the light, to modulate the amplitude and phase of the light. There are 400 pixels on the with 8 bits of resolution per pixel. The light is passed through the center 250 pixels.

The GA has a total of 42 genes each gene is an 8 bit value. Ten of the genes control amplitude terms and thirty-two control phase.

7.1.3 Experiment: Max. Absorption of Angular Momentum

Shaped ultrafast pulses have been used to control quantum dynamics of molecular systems. In this experiment, the goal was to accomplish the relatively simple task of putting angular momentum into our sample. In order to monitor the absorption of angular momentum, we used a pump-probe configuration.

The laser light coming out of the pulse shaper is at a 10Hz repetition rate. The width of the pulse is under 100 fs (femto 10^{-15} seconds). We used both 400 nm and 800 nm light with around 15nm of bandwidth for shaping. Each pulse is about 0.1 mJ. It's not really relevant, but if interpreted in watts, each pulse is 600 Megawatts over the pulse width.

7.1.4 Pump Probe Setup

The molecule we decided to pump, Coumarin 500, has a strong absorption peak from around 360 nm to 425 nm half-height full width.

Figure 7-2 is a diagram showing the basic setup for the 400 nm pumping experiment. Beginning on the left, the probe pulse is an unshaped pulse under 100 fs. A half-wave plate is used to rotate the polarization to a 45 degree angle from the normal of the plane of the table. We do this because at the very end we pass the light through a polarizing beam splitter. Linearly polarized light is composed of equal parts of left circularly-polarized light and right circularly-polarized light. The beam splitter will separate these components into two beams for comparison.

After the light passes through the half-wave plate, it is focused into a cuvette of water to generate a white light continuum. The probe beam is then passed through a polarizer at 45 degrees so that the maximum amount of light goes through. After the polarizer the light passes through the polished back of a mirror that has a dielectric coating that reflects only 400 nm. Since the frequency of the probe is now white, not much attenuation happens.

At this mirror, the white light is joined by the pump light that has been shaped by a GA. The pump has been delayed by a delay stage and then passed through a linear polarizer and then a quarter wave-plate to induce either right or left circular-polarization.

The two beams then proceed through the sample in a co-linear fashion. Hopefully at this point, the pump light is all absorbed by the sample. The sample is prepared to be optically dense at 400 nm. The probe light is then split by a polarizing beam splitter and

the two polarizations are observed by two photodiodes.

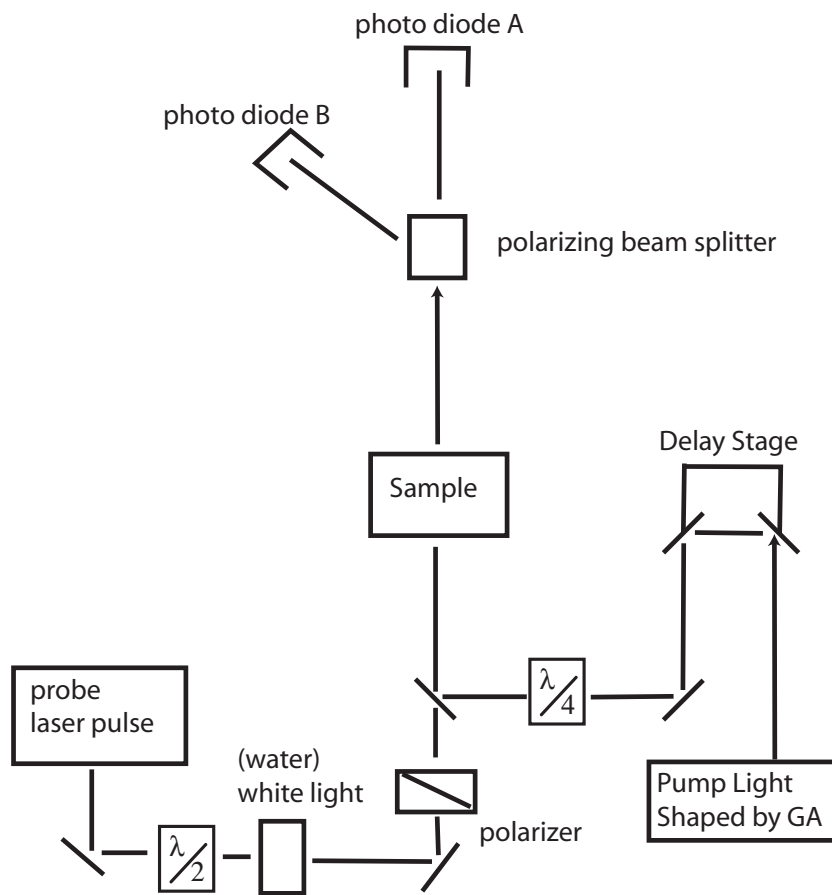


Figure 7-2: Pumping Schematic

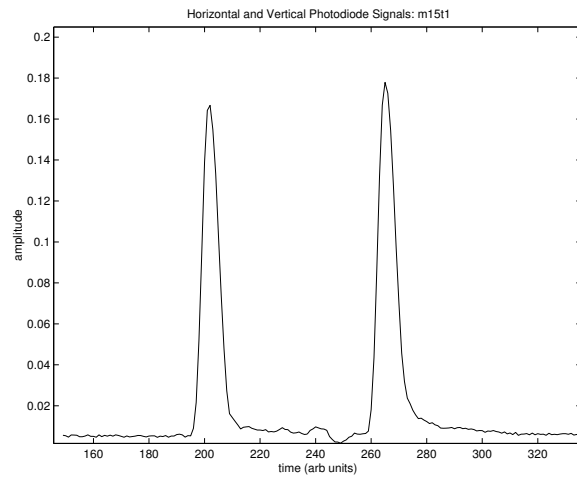


Figure 7-3: Photodiode trace

Time

Time resolution is the goal in a pump probe experiment. In general terms, the pump pulse will initiate a process and the probe will interrogate its progress. In the case of this experiment, a delay stage with a 40mm range was used. Because of the geometry this corresponds to a 80mm path difference for the light. This path difference is 260 ps (pico 10^{-12} seconds). The stepper was run at 0.2 ps per step.

If the center of the delay stage is where the pump and probe overlap in time in the sample ($t=0$), then if the pump has less of a delay than the delay at $t=0$, then it will come before the probe and if it has more of a delay, then it will come after the probe.

Figure 7-4 shows a plot of the fitness function as the pump is swept through the probe in time. The details of the fitness function are in the next section, but the feature to notice is the sharp drop in the center of the plot. This drop corresponds to $t=0$ where the pump and probe overlap in time. The data was taken in 208 fs steps which is large compared to the 100 fs pump-probe pulse widths.

Data Acquisition

The data from the photodiodes is used to determine how much of a particular polarization of light was absorbed by the probe. Figure 7-3 shows both photodiodes on the same oscilloscope trace. The one of the photodiodes had a longer cable than the other so that its signal was delayed in time.

The area under each peak corresponding to each photodiode is recorded. A fitness function was evaluated for each position of the delay stage,

$$\text{Fitness} = F_{left} = \frac{L - R}{L + R} \quad (7.1)$$

where L is the area under the left peak and R is the area under the right

$$\text{Fitness} = F_{right} = \frac{R - L}{L + R} \quad (7.2)$$

Figure 7-4 shows the fitness as a function of position of the delay stage. In this particular scan we were looking for the $t=0$ point to occur in the middle of the delay stage. The edge of the step function in the plot indicates the position of $t=0$ on the stage.

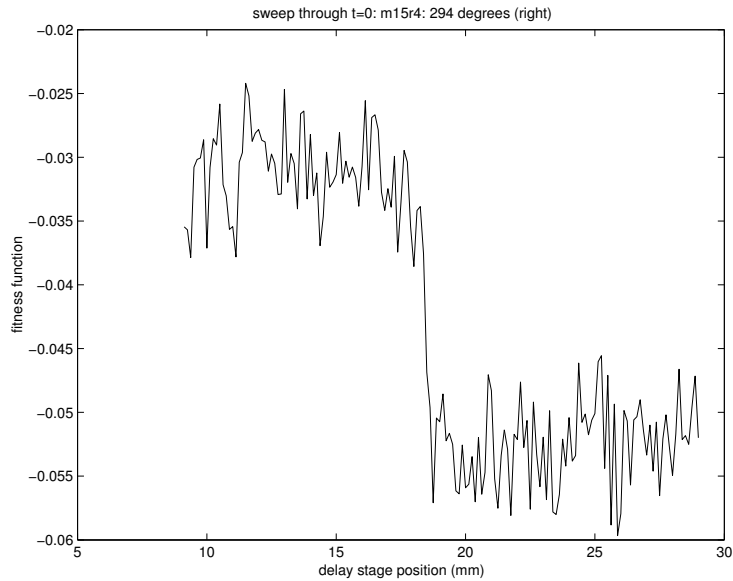


Figure 7-4: Fitness as the Pump Sweep is through the Probe (m15r4)

The Genetic Algorithm Run

The delay stage was then positioned so the pump preceded the probe by 4 mm in path length or 13 ps. The GA was then told to maximize the fitness function.

The ideal experiment is to have the GA run in four configurations.

- Left-Circularly polarized Pump and fitness of F_{right}
- Left-Circularly polarized Pump and fitness of F_{right}
- Right-Circularly polarized Pump and fitness of F_{left}
- Right-Circularly polarized Pump and fitness of F_{left}

Runs were done at 400 nm and 800 nm. The data will be discussed in the results section.

7.2 Progress and Results

Here we present the results and progress towards our goals. All of the optical data was collected by Daniel Morris in Phil Bucksbaum's group at the University of Michigan. The NMR related data was collected by Jason Taylor in Neil Gershenfeld's group at MIT.

The results were very positive. The experiments that we attempted produced reasonable and convincing results.

7.2.1 Results: Maximize Absorption of Angular Momentum

We have shown an improvement in the absorption of circularly-polarized light in our Coumarin 500 sample at both 400 nm and 800 nm.

For the purposes of this document we have arbitrarily labeled one circular-polarization left and the other right. The labeling is consistent throughout each experiment. The left and right channels were also arbitrarily labeled based on how the signals from the photodiodes changed when rotating the probe polarization.

800 nm Pump-Probe Experiment

This experiment was conducted as described in Section 7.1.3. This run attempts to maximize the absorption of 800 nm circularly polarized light pumping a Coumarin 500 sample. The Coumarin 500 sample doesn't absorb at 800 nm; this will be a two-photon absorption process.

There are two possible choices of fitness functions for left and right circularly-polarized (CP) light. The fitness functions correspond to trying to maximize the absorption of left or right circularly-polarized light.

In Figure 7-5 the GA attempted to maximize the left CP channel when pumping with left CP light. The GA was successful. Figures 7-6, 7-7 and 7-8 are the best pulse shapes for the last three generations of the GA run.

The plots are called Husimi plots. They are generated by taking the recorded input to the AOM and using calibration data taken just before the run to determine the resulting pulse shape. A Husimi plot is a Wigner function convolved with a Gaussian. The resulting Husimi plots show frequency in THz as a function of time in picoseconds.

If we examine only the first plot, Figure 7-6, it looks mostly like a transform limited

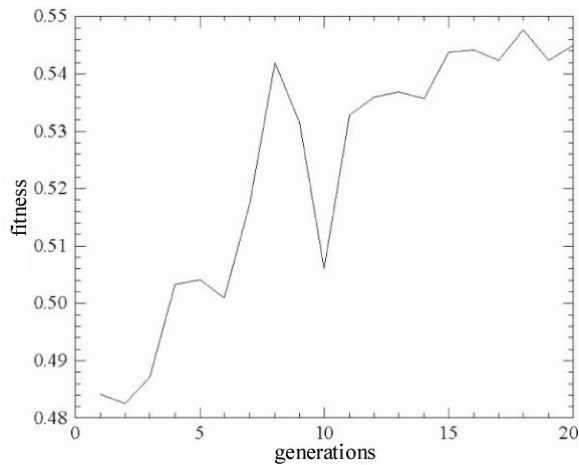


Figure 7-5: 800 nm pump. This GA seems to converge. The plot is of the best fitness in the group as a function of generation. The fitness was improved substantially indicating a good amount of control over the system.

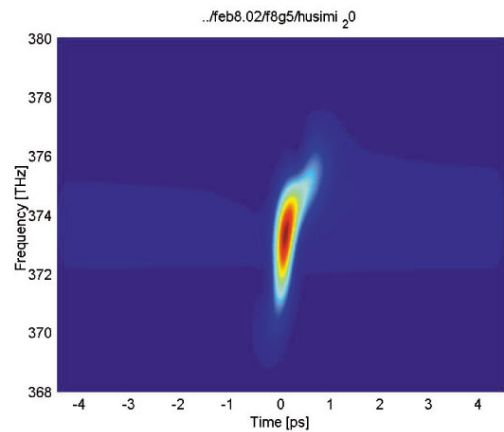


Figure 7-6: Husimi plot of the best pulse shape (generation 20); 800 nm pump

pulse. The pulse is vertical. If it were at a slight angle that would indicate a chirp in the pulse. The structure is consistent with what is seen when the GA corrects for imperfect compression of the beam¹.

The fact that this GA converged on a short intense pulse isn't too surprising since the mechanism for absorption is a two-photon process.

On the same day, using the same configuration, the GA was instructed to maximize the fitness for the other channel (the right channel for left light). This GA was not able to increase the fitness appreciably.

¹Observation by Daniel Morris, U. Mich.

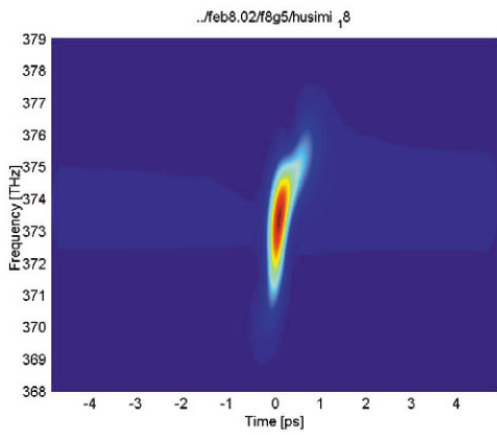


Figure 7-7: Husimi plot of the best pulse shape (generation 18); 800 nm pump

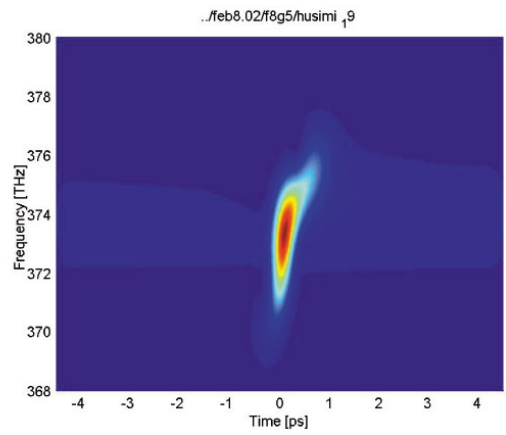


Figure 7-8: Husimi plot of the best pulse shape (generation 19); 800 nm pump

400 nm Pump-Probe Experiment

The 400 nm run went very well.

The four possible combinations of detecting on the left/right CP channel and pumping with left/right CP light all four were run and the GA performed well each time. Figures 7-9, 7-10, 7-11 and 7-12 contain the mean and average fitness functions for the pulses as a function of generation.

The resulting pulse shapes are shown in Figures 7-13 through 7-20. The pulses are all generally bandwidth limited pulses. The learning algorithm successfully improved the fitness function for the proper polarization by around 10% each time. This demonstrates that the shaped pulse was able to have some effect over a unshaped pulse. The fact that the pulse shapes are just short bandwidth limited pulses is not surprising considering our fitness function is based only on absorption of angular momentum. We expect much more interesting pulse shapes for the experiments proposed in Chapter 6.

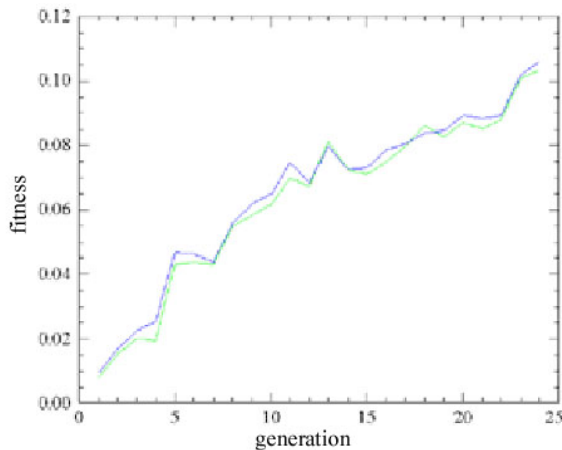


Figure 7-9: Converges; 400 nm pump; Maximize Right Channel; Right CP Pump; $\approx 10\%$ change

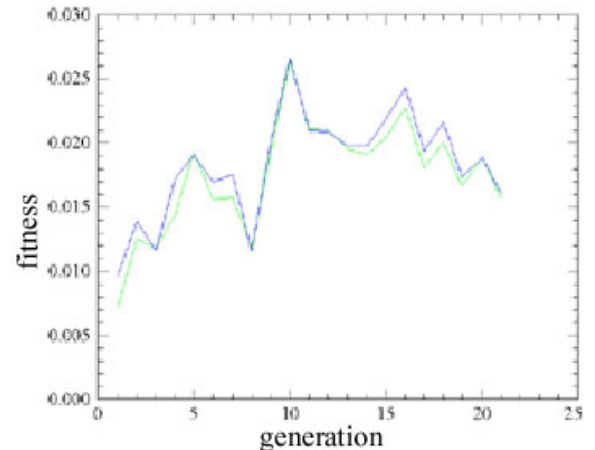


Figure 7-10: Small Improvement; 400 nm pump; Maximize Left Channel; Right CP Pump; $\approx 2\%$ change

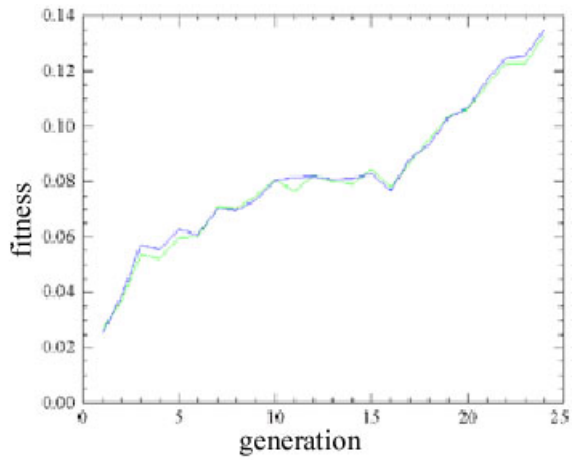


Figure 7-11: Converges; 400 nm pump; Maximize Left Channel; Left CP Pump; $\approx 10\%$ change

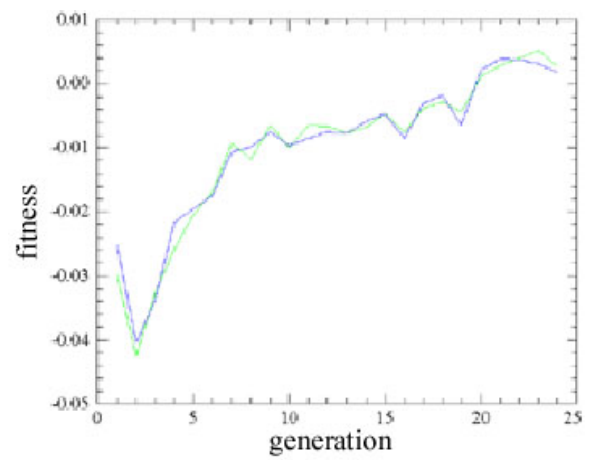


Figure 7-12: Small Improvement; 400 nm pump; Maximize Right Channel; Left CP Pump; $\approx 3\%$ change

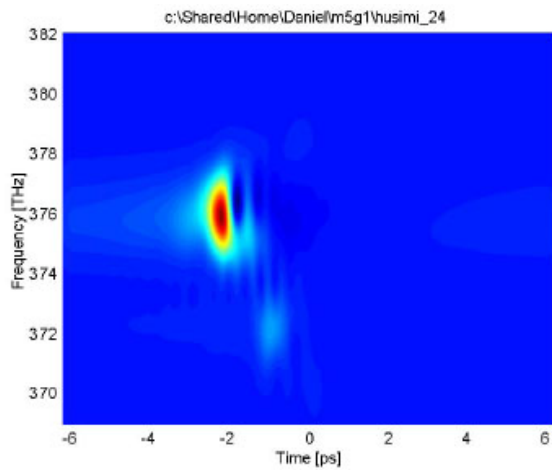


Figure 7-13: Right Channel; Right CP; Best pulse shape.

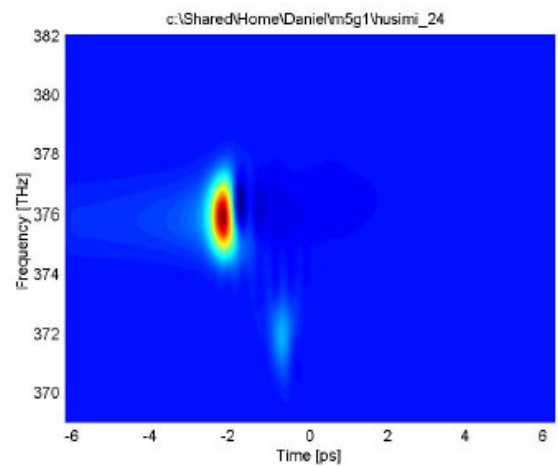


Figure 7-14: Right Channel; Right CP; Second Best pulse shape.

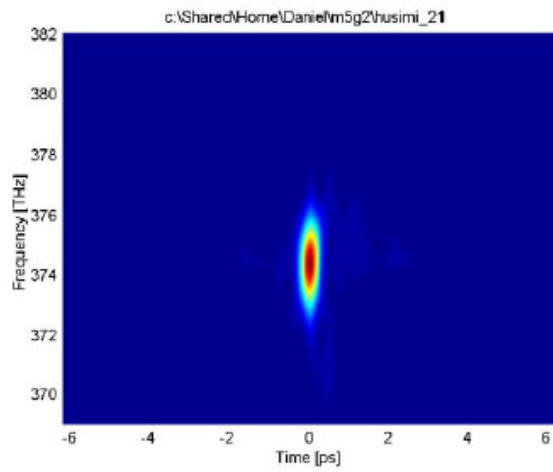


Figure 7-15: Left Channel; Right CP; Best pulse shape.

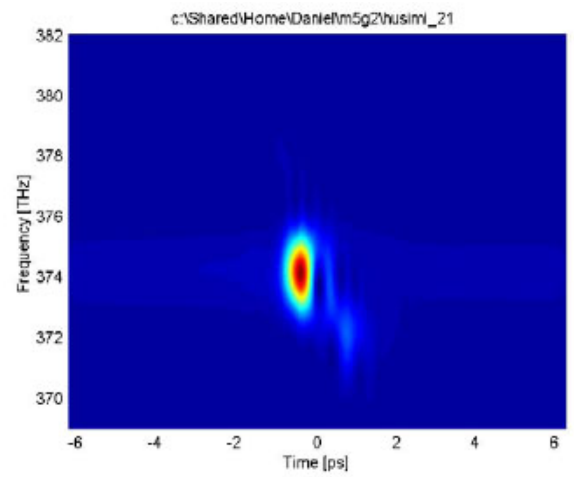


Figure 7-16: Left Channel; Right CP; Second Best pulse shape.

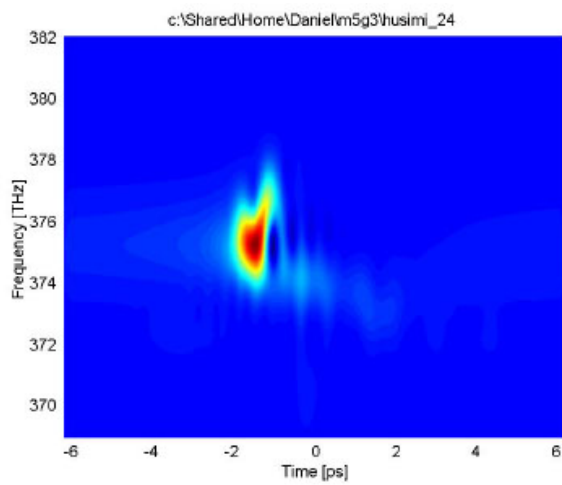


Figure 7-17: Left Channel; Left CP; Best pulse shape.

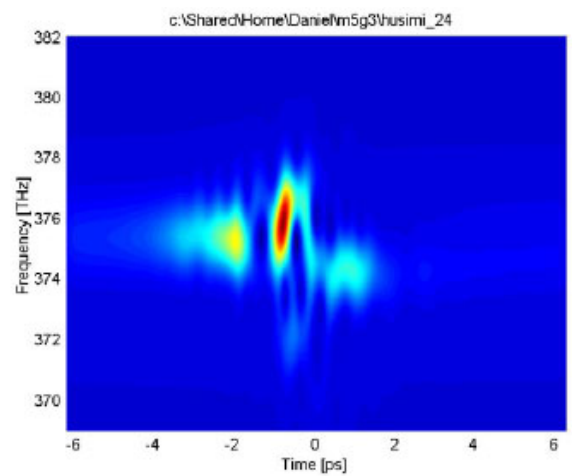


Figure 7-18: Left Channel; Left CP; Second Best pulse shape.

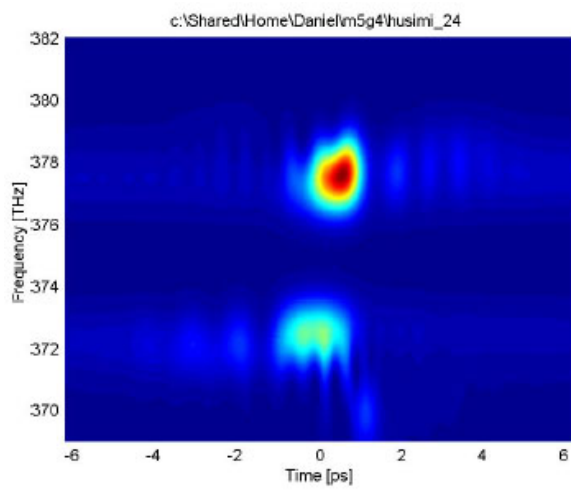


Figure 7-19: Right Channel; Left CP; Best pulse shape.

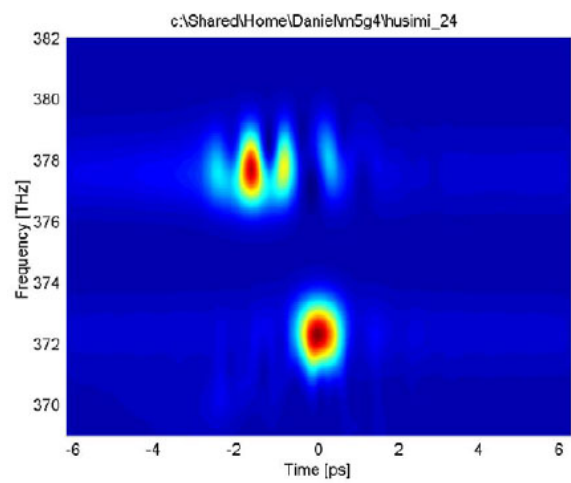


Figure 7-20: Right Channel; Left CP; Second Best pulse shape.

Chapter 8

Conclusions

We have presented here a good review of the fields related to shaped ultrafast pumping. The experimental exploration proved to be useful when deciding on what experiments might be possible for investigating shaped ultrafast optical pumping for NMR applications.

We have already begun implementing our proposed experiments. The initial data is encouraging. The next several weeks will occupy us with the plumbing necessary to integrate our laser pulse with our high resolution NMR.

The progress so far has been favorable enough for us to continue investigation in this research direction.

Appendix A

MO Simulation

Caveat Emptor.

These figures present the results of a molecular orbital simulation of the UV-VIS absorption spectra. The software package used is called CAChe. The predicted UV-VIS absorption spectra had the correct shape but the frequency axis was condensed. This is generally unacceptable and we will have to use a more sophisticated simulation package in order to be confident of the results. But, because the shape was correct, we have included these results.

Notice that for simulations for absorption points 10, 11, and 12 that correspond to 400nm, there is no activity around the Flourine atoms. We won't expect any polarization transfer from electrons involved in a 400nm absorption to the Flourine nuclei.

The surface is colored to indicate relative positive and negative areas of the HOMO. Negative areas are colored charcoal, violet, blue and cyan in increasing value. Positive areas are colored green, yellow, red, and white in increasing value.

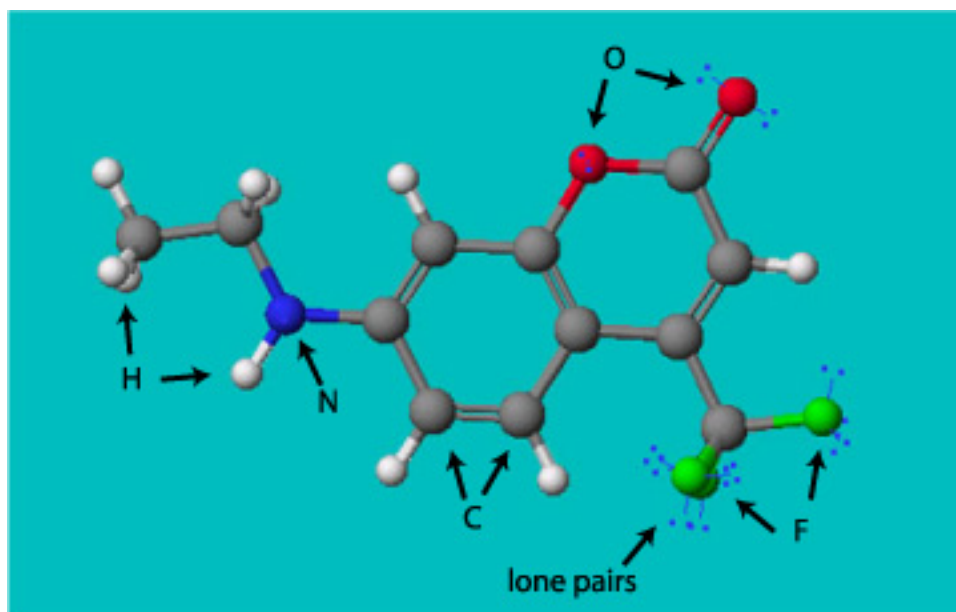


Figure A-1: Coumarin 500

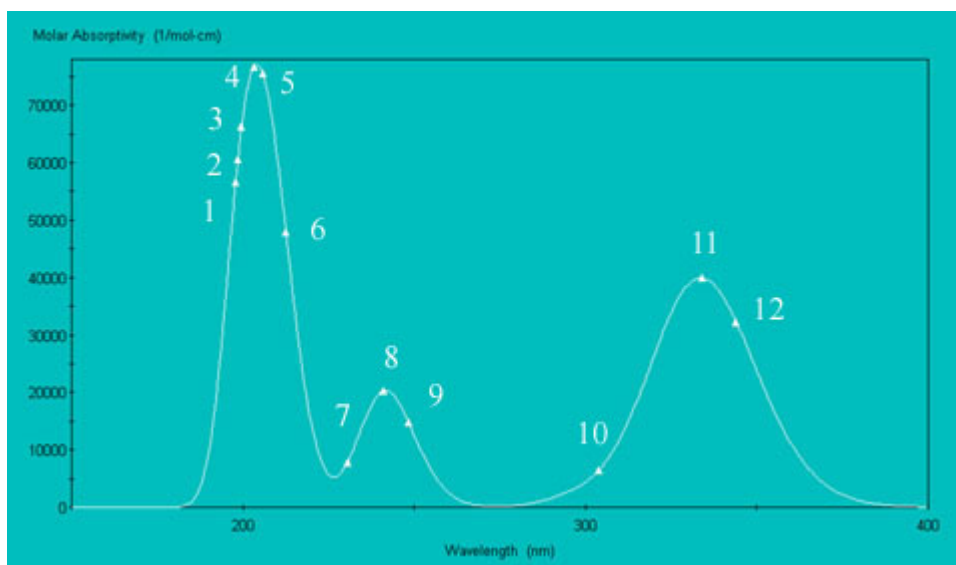


Figure A-2: Coumarin 500 UV-VIS simulation

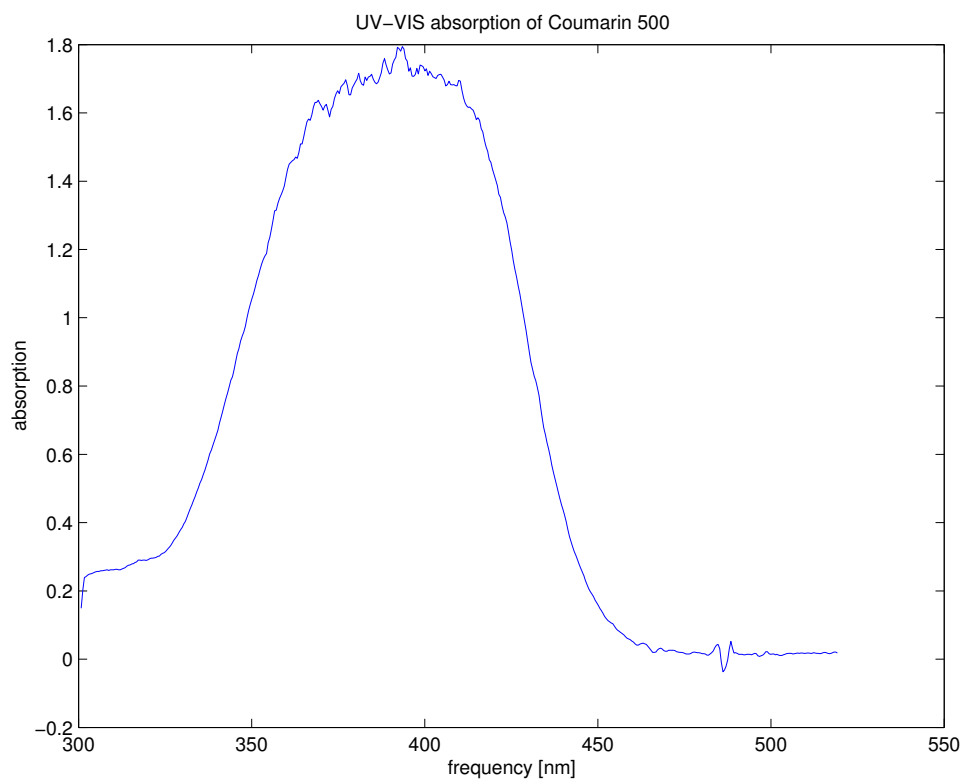


Figure A-3: Coumarin 500 UV-VIS simulation

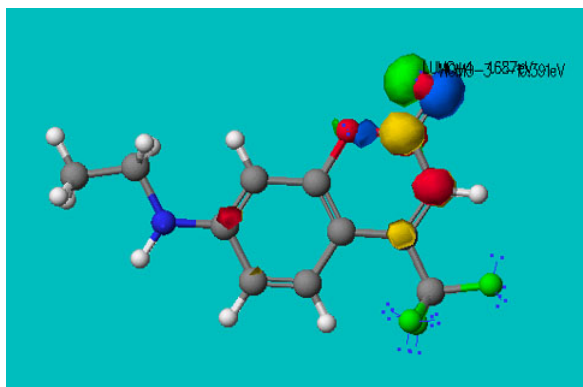


Figure A-4: Coumarin 500 point 1

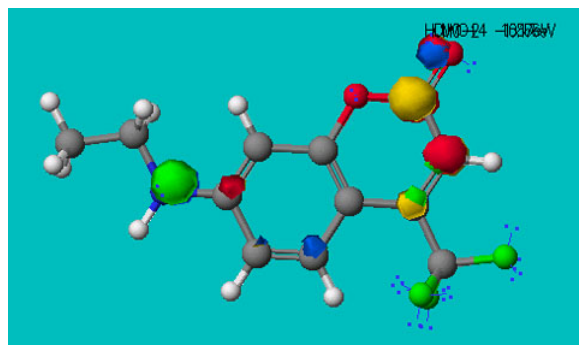


Figure A-5: Coumarin 500 point 2

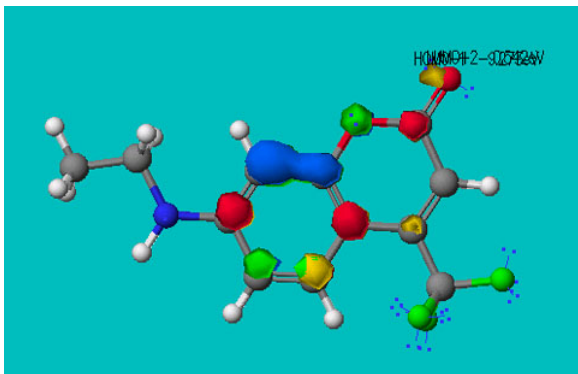


Figure A-6: Coumarin 500 point 3

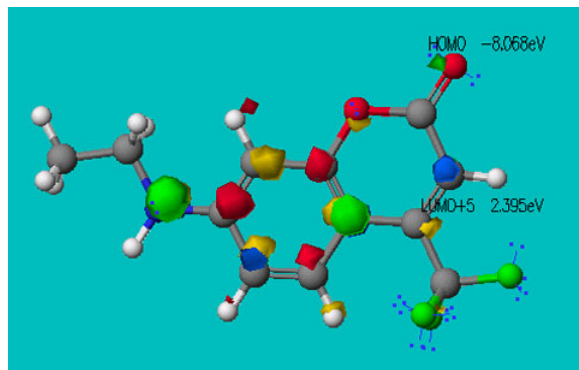


Figure A-7: Coumarin 500 point 4

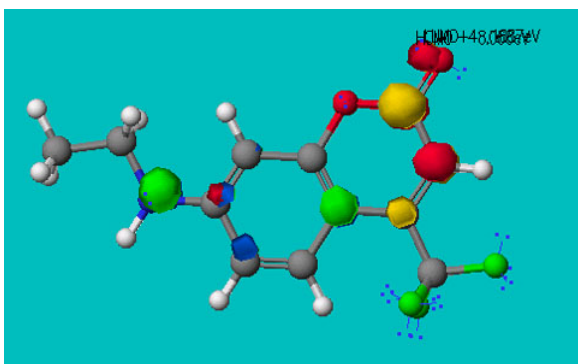


Figure A-8: Coumarin 500 point 5

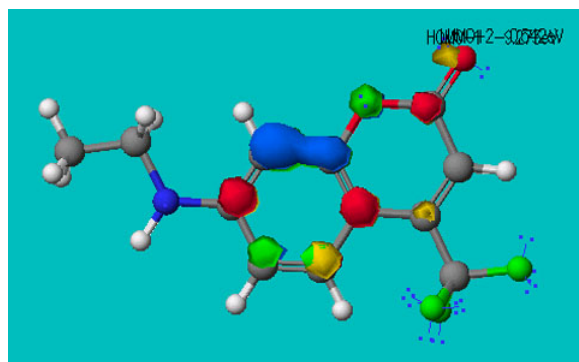


Figure A-9: Coumarin 500 point 6

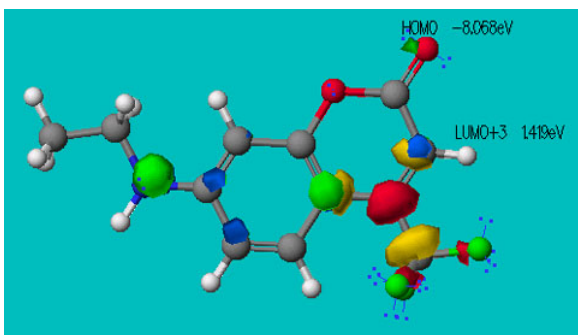


Figure A-10: Coumarin 500 point 7

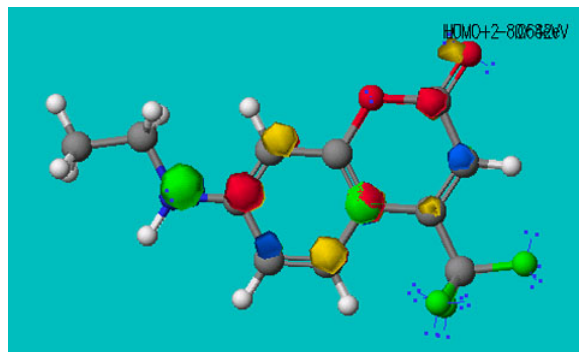


Figure A-11: Coumarin 500 point 8

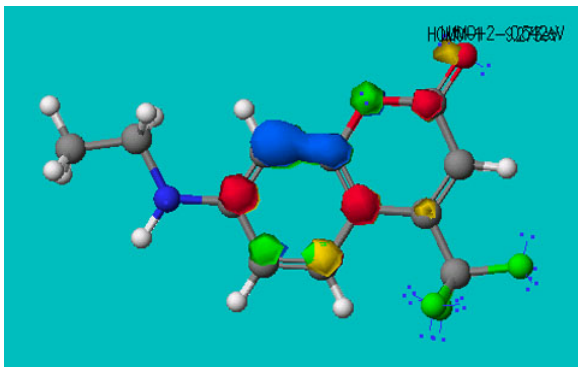


Figure A-12: Coumarin 500 point 9

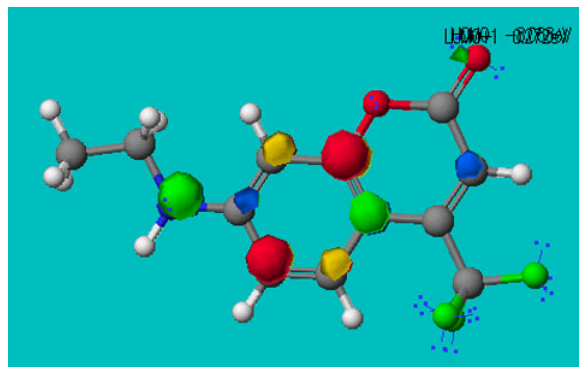


Figure A-13: Coumarin 500 point 10

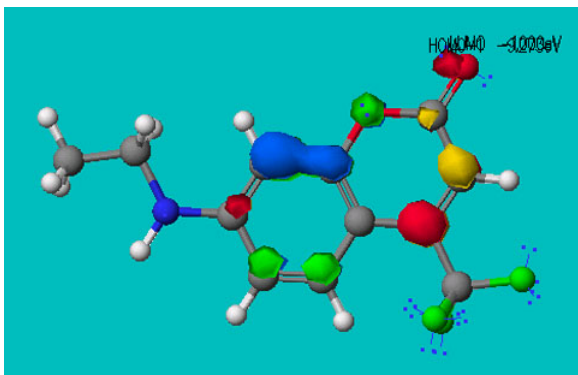


Figure A-14: Coumarin 500 point 11

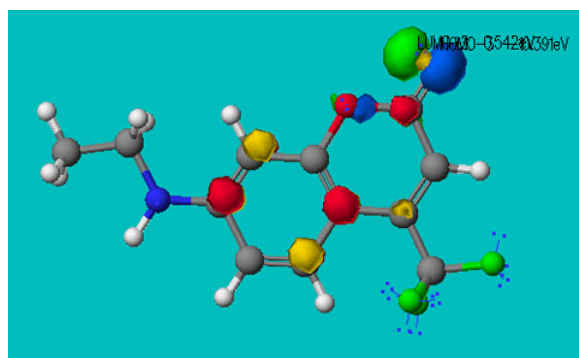


Figure A-15: Coumarin 500 point 12

Appendix B

Derivations with Spin

Here are some common derivations involving spin. They are helpful in becoming more comfortable.

B.1 Spin Operators

To introduce some notation [Gri95]: for a particular spin system, we have a value s that is the total spin of a system, and a value m that is the composite spin. If we have a $\frac{1}{2}$ spin particle and have decided on an orientation then we have two eigenstates:

$$|sm\rangle = \left| \frac{1}{2} \frac{1}{2} \right\rangle$$

and

$$|sm\rangle = \left| \frac{1}{2} \frac{-1}{2} \right\rangle$$

corresponding to spin up $|\uparrow\rangle$ and spin down $|\downarrow\rangle$. We can also define the spin operators:

$$[S_x, S_y] = i\hbar S_z$$

$$[S_y, S_z] = i\hbar S_x$$

$$[S_z, S_x] = i\hbar S_y$$

$$S^2|sm\rangle = \hbar^2 s(s+1)|sm\rangle$$

$$S_z|sm\rangle = \hbar m|sm\rangle$$

and the raising and lowering operators:

$$S_{\pm}|sm\rangle = \hbar\sqrt{s(s+1) - m(m\pm 1)}|s(m\pm 1)\rangle$$

$$S_{\pm} \equiv S_x \pm iS_y$$

Using these operators then we have values for s and m :

$$s = 0, \frac{1}{2}, 1, \frac{3}{2}, 2, \dots$$

$$m = -s, -s+1, \dots, s-1, s$$

B.2 Two $\frac{1}{2}$ Spins

Spin operators are pretty exciting. Let's now consider the energy levels of a two spin system. We won't have any magnetic field here, just a proton and an electron in the ground state. Both the proton and electron are spin $\frac{1}{2}$ particles. For this section, we will be following Griffiths [Gri95]. There will be no uniform magnetic field here.

With two spins they will be either aligned or anti-aligned. This gives us four possibilities.

$$\uparrow\uparrow, \downarrow\uparrow, \uparrow\downarrow, \downarrow\downarrow$$

The composite spin of this system (the Z component) is:

$$\uparrow\uparrow: m = 1$$

$$\downarrow\uparrow: m = 0$$

$$\uparrow\downarrow: m = 0$$

$$\downarrow\downarrow: m = -1$$

(B.1)

What is the total angular momentum? Since $m=\pm 1$ then $s = 0, 1$.

The two middle values of $m = 0$ are a bit confusing. Let's apply a lowering operator to the $|1, 1\rangle = \uparrow\uparrow$ state in order to find out what the $|1, 0\rangle$ state is. We'll continue to follow Griffiths.

For two spins the spin operator S is defined by

$$S = S^{(1)} + S^{(2)}$$

and it is easy to show that it obeys the commutation relationships.

$$\begin{aligned} S_-(\uparrow\uparrow) &= (S_-^{(1)} \uparrow) \uparrow + \uparrow (S_-^{(2)} \uparrow) \\ &= (\hbar \downarrow) \uparrow + \uparrow (\hbar \downarrow) = \hbar(\downarrow\uparrow + \uparrow\downarrow) \end{aligned} \tag{B.2}$$

The three states with $s=1$:

$$\begin{aligned} |1, 1\rangle &= \uparrow\uparrow \\ |1, 0\rangle &= \frac{1}{\sqrt{2}}(\uparrow\downarrow + \downarrow\uparrow) \\ |1 - 1\rangle &= \downarrow\downarrow \end{aligned} \tag{B.3}$$

and one state with $s=0$:

$$|0, 0\rangle = \frac{1}{\sqrt{2}}(\uparrow\downarrow - \downarrow\uparrow)$$

The three states are called a triplet and the $s=0$ state is called a singlet.

B.2.1 Clebsch-Gordan Coefficients

From the spin operators one can derive the Clebsch-Gordan Coefficients. Rather than use $|sm\rangle$ we'll change to the more common notation of $|JM\rangle$ where J is our total angular momentum and as used in [ST95] and [AW95]. M is the total composite spin in the Z direction. For a particular $|JM\rangle = |1, 1\rangle$ the CG coefficients give us:

$$|2, 0\rangle = \sqrt{\frac{1}{6}}|1(-1)\rangle + \sqrt{\frac{2}{3}}|0, 0\rangle + \sqrt{\frac{1}{6}}|(-1)1\rangle$$

If we do a measurement on this $S_Z|2, 0\rangle$ then we'll get $2\hbar$ with a probability $\sqrt{\frac{1}{6}}$, or \hbar with a probability of $\sqrt{\frac{2}{3}}$, or 0 with a probability of $\sqrt{\frac{1}{6}}$.

B.3 spin $\frac{1}{2}$

We will now see how far some quantum mechanics can take us. We will follow Cohen-Tannoudji [CTDL77].

B.4 Spin in a magnetic field

If we have a spin $\frac{1}{2}$ particle like a proton or electron, in a uniform magnetic field, B_0 , then we can consider the interaction with the magnetic moment $\vec{\mu}$.

If the spin, \vec{S} , is aligned with the field then we have for the Z component an operator:

$$S_Z = \begin{pmatrix} 1 & 0 \\ 0 & -1 \end{pmatrix}$$

This can result in only two eigenstates:

$$S_Z |\uparrow\rangle = +\frac{\hbar}{2} |\uparrow\rangle$$

$$S_Z |\downarrow\rangle = -\frac{\hbar}{2} |\downarrow\rangle$$

For the magnetic moment of the spin:

$$\vec{\mu} = \gamma \vec{S}$$

Where γ is the gyromagnetic ratio for the particle.

$$E = -\vec{\mu} \cdot \vec{B}_0 = \gamma S_Z B_0$$

We can define:

$$\omega_0 = -\gamma B_0$$

So, if we want to describe the evolution of this particle then we'll have the Hamiltonian:

$$H = \hbar \omega_0 S_Z$$

If we then look at the eigenvectors of H :

$$H|\uparrow\rangle = +\frac{\hbar\omega_0}{2}|\uparrow\rangle$$

$$H|\downarrow\rangle = -\frac{\hbar\omega_0}{2}|\downarrow\rangle$$

So we have two energy levels.

$$E_+ = +\frac{\hbar\omega_0}{2}$$

$$E_- = -\frac{\hbar\omega_0}{2}$$

for an energy difference of

$$\Delta E = \hbar\omega$$

B.5 The Larmor Precession

We can write down a general vector for the above system representing a superposition of the aligned/anti-aligned state.

$$|\Psi\rangle = \alpha|\uparrow\rangle + \beta|\downarrow\rangle$$

and

$$|\alpha|^2 + |\beta|^2 = 1$$

A time independent solution is:

$$\alpha = \cos\left(\frac{\theta}{2}\right) \exp\left(-\frac{i\phi}{2}\right)$$

$$\beta = \sin\left(\frac{\theta}{2}\right) \exp\left(\frac{i\phi}{2}\right)$$

$$|\Psi(0)\rangle = \cos\left(\frac{\theta}{2}\right) \exp\left(-\frac{i\phi}{2}\right) |\uparrow\rangle + \sin\left(\frac{\theta}{2}\right) \exp\left(\frac{i\phi}{2}\right) |\downarrow\rangle$$

Then we can apply the time evolution operator.

$$\exp\left(-\frac{iHt}{\hbar}\right) |\Psi(0)\rangle = |\Psi(t)\rangle$$

If we use the values of E_+ and E_- (still following closely [CTDL77])

$$|\Psi(t)\rangle = \cos\left(\frac{\theta}{2}\right) \exp\left(-i\frac{\phi + \omega_0 t}{2}\right) |\uparrow\rangle + \sin\left(\frac{\theta}{2}\right) \exp\left(i\frac{\phi + \omega_0 t}{2}\right) |\downarrow\rangle$$

So our variables are a position vector θ defined along the Z axis, and a ω_0 rotation term with a phase ϕ . The ω_0 is proportional to the magnetic field and is known as the Larmor Frequency.

Appendix C

Glossary

[CP] Cross Polarization

[CPMG] Carr-Purcell-Meiboom-Gill; NMR pulse sequence to determine T_2

[CIDNP] Chemically Induced Dynamic Nuclear Polarization

[COSY] COrrrelation SpectroscopY

[DNP] Dynamic Nuclear Polarization

[FID] Free Induction Decay

[ENDOR] Electron-Nuclear DOuble Resonance

[ELDOR] Electron eLectron DOuble Resonance

[FWHM] Full Width at Half Maximum

[IR] Inversion Recovery

[INDOR] INternuclear DOuble Resonance

[INEPT] Insensitive Nucleus Enhancement by Polarization Transfer

[INADEQUATE] Incredible Natural Abundance Double-QUantum Transfer Experiment

[NOESY] Nuclear Overhauser and Exchange SpectroscopY

[NOE] Nuclear Overhauser Effect

[DARPA] Defense Advanced Research Projects Agency

[HETCOR] HEteronuclear chemical-shift CORrelation

[HOESY] Heteronuclear Overhauser Enhancement Spectroscopy

[HOMO] Highest Occupied Molecular Orbital

[NAR] Nuclear Acoustic Resonance

[NMR] Nuclear Magnetic Resonance

[ONP] Optical Nuclear Polarization

[SNR] Signal to Noise Ratio

Bibliography

- [AW95] George B. Arfken and Hans J. Weber. *Mathematical methods for physicists*. Academic Press Inc., San Diego, CA, fourth edition, 1995.
- [BDNG01] T. Brixner, N.H. Damrauer, P. Niklaus, and G. Gerber. Photosensitive adaptive femtosecond quantum control in the liquid phase. *Nature*, 414:57–60, 2001.
- [CAGPFS96] John Cavanagh, III Arthur G. Palmer, Wayne Fairbrother, and Nicholas Skelton. *Protein NMR Spectroscopy*. Academic Press, New York, 1996.
- [CGK98] I.L. Chuang, N. Gershenfeld, and M. Kubinec. Experimental implementation of fast quantum searching. *Phys. Rev. Lett.*, 80:3408–3411, 1998.
- [Cor77] Alan Corney. *Atomic and Laser Spectroscopy*. Clarendon Press, Oxford, 1977.
- [CP97] Jr. Charles Poole. *ELECTRON SPIN RESONANCE A Comprehensive Treatise on Experimental Techniques*. Dover Publications, Inc., Mineola, NY, 1997.
- [CS01] T. Chupp and S. Swanson. Medical imaging with laser-polarized noble gasses. *Advances in Atomic, Molecular, and Optical Physics*, 45:41, 2001.
- [CTDL77] Claude Cohen-Tannoudji, Bernard Diu, and Franck Laloe. *Quantum Mechanics, Volume 1*. John Wiley and Sons, New York, 1977.
- [CVZ⁺98] I.L. Chuang, L.M.K. Vandersypen, Xinlan Zhou, Debbie W. Leung, and Seth Lloyd. Experimental realization of a quantum algorithm. *Nature*, 393:143, 1998.

- [EBW97] R. R. Ernst, G. Bodenhausen, and A. Wokaun. *Principles of Nuclear Magnetic Resonance in One and Two Dimensions*. Oxford University Press, Oxford, UK, 1997.
- [For93] Stephanie Forrest. Genetic algorithms: Principles of natural selection applied to computation. *Science*, 261:872–78, 1993.
- [FR81] Eiichi Fukushima and Stephen B.W. Roeder. *Experimental Pulse NMR: A Nuts and Bolts Approach*. Addison-Wesley, Reading, 1981.
- [Fre97] Ray Freeman. *Spin Choreography*. Spektrum Academic Publishers, 33 Beaumont Street, Oxford OX1 2PF, 1997.
- [GB91] Andrew Gilbert and Jim Baggott. *Essentials of Molecular Photochemistry*. Blackwell Scientific Publications, London, 1991.
- [Ger99] Neil Gershenfeld. *The nature of mathematical modeling*. Cambridge University Press, Cambridge, 1999.
- [Gri95] David J. Griffiths. *Introduction to Quantum Mechanics*. Prentice Hall, Upper Saddle River, New Jersey 07458, 1995.
- [Gro97a] Lov K. Grover. Quantum computer can search arbitrarily large databases by a single query. *Physical Review Letters*, 79:4709–4712, 1997.
- [Gro97b] Lov K. Grover. Quantum mechanics helps in searching for a needle in a haystack. *Physical Review Letters*, 79:325–328, 1997.
- [Hap72] William Happer. Optical pumping. *Reviews of Modern Physics*, 44(2):169–249, 1972.
- [HB89] Daniel Harris and Michael Bertolucci. *Symmetry and Spectroscopy: An Introduction to Vibrational and Electronic Spectroscopy*. Dover Publications, Inc., New York, 1989.
- [Hor97a] Joseph P. Hornak. The basics of nmr. <http://www.cis.rit.edu/htbooks/nmr/>, 1997.

- [Hor97b] J.P. Hornak. The basics of nmr. <http://www.cis.rit.edu/htbooks/nmr/>, 1997.
- [IAK00] Kazuyuki Ishii, Satoko Abiko, and Nago Kobayashi. Time-resolved electron spin resonance of gallium and germanium porphyrins in the excited triplet state. *Inorganic Chemistry*, 39:468–472, 2000.
- [ITS⁺00] M. Iinuma, Y. Takahashi, I. Shake, M. Oda, A. Masaike, and T. Yabuzaki. High proton polarization by microwave-induced optical nuclear polarization at 77k. *Physical Review Letters*, 84(1):171–174, 2000.
- [Jef63] Carson D. Jeffries. *Dynamic Nuclear Orientation*. Interscience Publishers a division of John Wiley and Sons, New York, 1963.
- [Kra96] Kenneth S. Krane. *Modern Physics*. John Wiley and Sons, New York, 1996.
- [LP02] Inc. Lambda Physik. Lambdachrome laser dyes book. http://www.lambdaphysik.com/pdf/pdf_54.pdf, 2002.
- [Mag99] Yael Maguire. Towards a table top quantum computer. Masters Thesis, MIT Media Lab, 1999.
- [Moo65] Gordon Moore. Cramming more components onto integrated circuits. *Electronics*, 38(8), 1965.
- [NC00] M. A. Nielsen and I. L. Chuang. *Quantum Computation and Quantum Information*. Cambridge University Press, Cambridge, UK, 2000.
- [PM99] Tatyana Polenova and Ann McDermott. A coherent mixing mechanism explains the photoinduced nuclear polarization in photosynthetic reaction centers. *J. Phys. Chem. B*, 103:535–548, 1999.
- [PTP46] E. M. Purcell, H. C. Torrey, and R. V. Pound. Resonance absorption by nuclear magnetic moments in a solid. *Phys. Rev.*, 69:37, 1946.
- [PWWB01] B.J. Pearson, J.L. White, T.C. Weinacht, and P.H. Bucksbaum. Coherent control using adaptive learning algorithms. <http://xxx.lanl.gov/abs/quant-ph/0008029>, 2001.

- [RdVRMK00] Herschel Rabitz, Regina de Vivie-Riedle, Marcus Motzkus, and Karl Kompa. Whither the future of controlling quantum phenomena? *Science*, 288:824–8, 2000.
- [SEL⁺83] O.W. Sorensen, G.W. Eich, M.H. Levitt, G. Bodenhausen, and R.R. Ernst. Product operator formalism for the description of nmr pulse experiments. *Progress in NMR Spectroscopy*, 163:163–192, 1983.
- [Sho95] P.W. Shor. Polynomial-time algorithms for prime factorization and discrete logarithms on a quantum computer. <http://xxx.lanl.gov/abs/quant-ph/9508027>, 1995.
- [SPHR99] R. Seydoux, A. Pines, M. Haake, and J.A. Reimer. Nmr with a continuously circulating flow of laser-polarized ¹²⁹xe. *J. Phys. Chem. B*, 103:4629–4637, 1999.
- [ST95] Klaus Schertler and Markus H. Thoma. Combinatorial computation of clebsch-gordan coefficients. <http://xxx.lanl.gov/abs/quant-ph/9504015>, 1995.
- [SV98] L. Shulman and U. Vazirani. Scalable nmr quantum computation. <http://xxx.lanl.gov/abs/quant-ph/9804060>, 1998.
- [VSB⁺00] Lieven M.K. Vandersypen, Matthias Steffen, Gregory Breyta, Costantino S. Yannoni, Richard Cleve, and Isaac L. Chuang. Experimental realization of an order-finding algorithm with an nmr quantum computer. *Physical Review Letters*, 85(25):5452, 2000.
- [War97] W.S. Warren. On the practicality of nmr quantum computing. *Science*, 277:1688, 1997.
- [WC98] Colin P. Williams and Scott H. Clearwater. *Explorations in Quantum Computing*. Telos, New York, NY, 1998.
- [WH97] Thad G. Walker and William Happer. Spin-exchange optical pumping of noble-gas nuclei. *Reviews of Modern Physics*, 69(2):629–642, 1997.

- [Zew00] Ahmed H. Zewail. Femtochemistry: Atomic-scale dynamics of the chemical bond. *J. Phys. Chem. A*, 104:5660–5694, 2000.
- [ZM94] Martin G. Zysmilich and Ann McDermott. Photochemically induced dynamic nuclear polarization in the solid-state ^{15}N spectra of reaction centers from photosynthetic bacteria rhodobacter sphaeroides r-26. *J. Am. Chem. Soc.*, 116:8362–8363, 1994.
- [ZM96] Martin G. Zysmilich and Ann McDermott. Photochemically induced nuclear spin polarization in bacterial photosynthetic reaction centers: Assignments of the ^{15}N ssnmr spectra. *J. Am. Chem. Soc.*, 118:5867–5873, 1996.